



Magnetic anisotropy of an ancient volcanic system: Flow dynamics of post-collisional Ediacaran volcanism in southernmost Brazil

Johnathan H. Gambeta^{a,*}, Jairo F. Savian^a, Carlos A. Sommer^a, Ricardo I.F. Trindade^b

^a Instituto de Geociências, Universidade Federal do Rio Grande do Sul, Av. Bento Gonçalves, 9500, Porto Alegre, Rio Grande do Sul, Brazil

^b Departamento de Geofísica, Instituto de Astronomia, Geofísica e Ciências Atmosféricas, Universidade de São Paulo, Rua do Matão, 1226 São Paulo, Brazil

ARTICLE INFO

Keywords:

Neoproterozoic volcanism
Anisotropy of magnetic susceptibility
Anisotropy of anhysteretic remanent magnetization
Magnetic fabric
Lava flow dynamics
Rock magnetism

ABSTRACT

Knowledge about flow dynamics of volcanic sequences is fundamental for understanding their emplacement and consequently the evolution of the associated volcanic terrain. Despite this importance, studies that apply different approaches to ancient volcanic systems are still rare. In this paper, we study the case of silicic volcanic sequences in southernmost Brazil, contributing to the interpretation of the post-collisional Ediacaran volcanic settings of the Sul-riograndense shield. Rock magnetism analyses, anisotropy of magnetic susceptibility (AMS) and anisotropy of anhysteretic remanent magnetization (AARM), were performed on 32 sites of silicic volcanic rocks integrated with fieldwork observations. Magnetic mineralogy data indicate that magnetite or Ti-poor magnetite and high-coercivity phases (e.g., hematite) are the main magnetic carriers for the studied volcanic deposits. AARM results reveal an inverse magnetic fabric when single-domain grains are present, strongly affecting the interpretation of flow directions of lavas and ignimbritic deposits. AMS scalar results integrated with ignimbrite lithofacies analyses showed different fabric imbrication styles between stratified lower units and rheomorphic upper ignimbrites, allowing their separation in the emplacement model. Flow directions based on AMS, AARM data and field observations show a potential correlation of these volcanic deposits with an intrusive complex located on the southeastern border of the ignimbritic plateau. The emplacement of pyroclastic flow deposits was probably associated with a complex fissure system, where discontinuities within the basement plateau border may have served as feed conduits for these deposits. Our results highlight the importance of applying a regionally distributed AMS sampling coupled with a strong mineralogical and field control to the study of ancient volcanic systems.

1. Introduction

The analysis of ancient volcanic terrains is essential for understanding the evolution of post-tectonic volcanism in orogenic belts. Presently, most studies on the behaviour of volcanic systems are related to the observation of modern or recent erupting systems (e.g., Newhall et al., 2000; Jousset et al., 2012). Yet, the mechanisms and flow dynamics of acidic volcanic sequences, mainly pyroclastic deposits, are still in a subject of debate in the literature (e.g., Alva-Valdivia et al., 2017; Lima et al., 2018). In this context, a detailed examination of particle fabric in rocks of ancient acidic volcanic deposits may provide insights into their transport and deposition, which is fundamental to interpret the volcanic emplacement.

In southern Brazil, acidic orogenic volcanism is well exposed and offers the opportunity to a better understanding of their flow dynamics.

The Ediacaran to Ordovician Camaquã Basin (CB) is a well preserved volcano-sedimentary molassic basin (Paim et al., 2000, 2014), associated to the complex evolution of the Sul-riograndense shield (Fig. 1), formed in the late to post-collisional stages of the Brasiliano cycle of the Dom Feliciano belt (Sommer et al., 2006; Hartmann et al., 2007; Paim et al., 2014). There is no evidence of ductile deformation and associated metamorphism in the CB, favouring studies of ancient volcanic systems due to the exquisite preservation of their primary structures. This basin is divided into sub-basins, whose tectonic environments indicate a retroarc setting evolving into a strike-slip and ending as a transtensive rift (Chemale, 2000; Frago-Cesar et al., 2000; Paim et al., 2000, 2014).

Present in the Taquarém sub-basin (Paim et al., 2014), the Taquarém Plateau (TP) preserves silicic volcanic sequences, mainly pyroclastic deposits, characterized by a non-deformed and non-metamorphosed succession with only slight brittle tectonics, known as

* Corresponding author.

E-mail address: johnathan.gambeta@ufrgs.br (J.H. Gambeta).

<https://doi.org/10.1016/j.precamres.2021.106209>

Received 27 October 2020; Received in revised form 30 March 2021; Accepted 30 March 2021

Available online 18 April 2021

0301-9268/© 2021 Elsevier B.V. All rights reserved.

the Acampamento Velho Formation (AVF; Ribeiro and Fantinel, 1978). This unit is characterized by subhorizontal ignimbrites that preserve features typical of primary pyroclastic processes indicative of high temperature flows with a large amount of gases. These attributes, combined with the frequent occurrence of lavas and synvolcanic bodies, suggest subaerial volcanism, probably related to the fissure vents and volcanic calderas (Sommer et al., 1999, 2011, 2013).

Acquiring directional data of lava and pyroclastic flows is fundamental to identify the sources for volcanic deposits. The analysis of structural and textural data (e.g., flow foliations, mineral lineation, imbricated logs including orientation of glass shards, crystals, pumice and lithic fragments), is time consuming and these features are commonly absent in specific outcrops (e.g., Dedzo et al., 2011). Many

authors have used indirect methods, such as anisotropy of magnetic susceptibility (AMS) and anisotropy of anhysteretic remanent magnetization (AARM) measurements, to assist in these studies (e.g., Inoronato et al., 1983; Ort, 1993; Fisher et al., 1993; Cagnoli and Tarling, 1997; Le Penec et al., 1998; Palmer and MacDonald, 1999; Ort et al., 1999; LaBerge et al., 2009). AMS is a powerful tool for volcanic studies because it permits determining the preferred orientation of the magnetic minerals present in the rocks during their formation (e.g., Graham, 1954; Tarling and Hrouda, 1993). Despite its strong potential, case studies using AMS and AARM in Precambrian volcanic systems are still rare.

Here we propose to identify sources for volcanic deposits in the Taquarembó plateau region, in order to indicate and discuss the transport mechanisms and flow dynamics of these sequences, assisting with

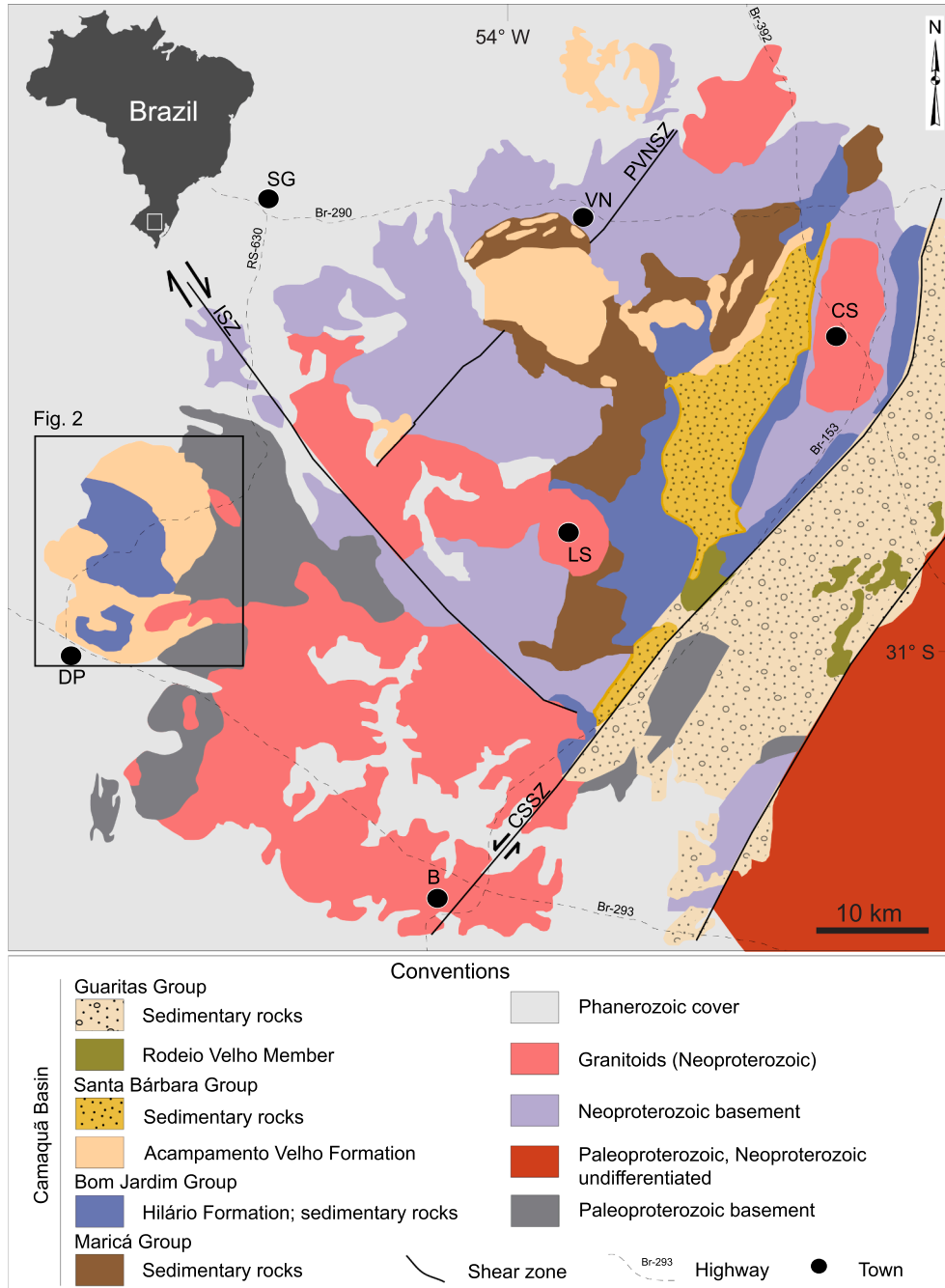


Fig. 1. Regional map with location of the study area. Towns: B = Bagé; CS = Caçapava do Sul; DP = Dom Pedrito; LS = Lavras do Sul; SG = São Gabriel; VN = Vila Nova do Sul. Shear zones: ISZ = Ibaré; CSSZ = Caçapava do Sul; PVNSZ = Passinho/Vila Nova do Sul. Neoproterozoic granitoids are coeval with the Camaquã Basin (Modified from Philipp et al., 2016; Cerva-Alves et al., 2020).

their emplacement characterization. This information, linked with data from this unit in other exposures in the Sul-riograndense shield, contributes to the interpretation of the post-collisional Ediacaran volcanism in Dom Feliciano belt. To attain this objective, we obtained directional data of lava and ignimbrites using AMS and AARM measurements integrated with rock magnetism analyses and fieldwork observations. This study demonstrates how this approach may be used not only to reconstruct modern volcanic systems but also to elucidate important scientific questions related to ancient volcanic events around the world.

2. Geological setting

The Camaquã Basin is characterized by volcano-sedimentary sequences deposited between about 620 and 540 Ma (Paim et al., 2014)

associated with the final stages of evolution of the Sul-riograndense Shield in southernmost Brazil. The basin basement is heterogeneous and varies from Paleoproterozoic metamorphic terrains (e.g. Santa Maria Chico Granulitic Complex) to Neoproterozoic units represented by igneous and metamorphic associations (Fig. 1) (Paim et al., 2000; Lima et al., 2007).

Concerning the geological evolution of CB, it represents a depositional locus, characterized by an interleaving of events with the accumulation of sedimentary and volcano-sedimentary sequences, and erosional intervals (Paim et al., 2000). Volcanic deposits occur predominantly at the base of the units with subsequent deposition of mainly siliciclastic sediments. The dynamic context of CB resulted in a complex filling pattern, linked to different tectonic environments, whose records are limited by angular discordances, organized in a series of

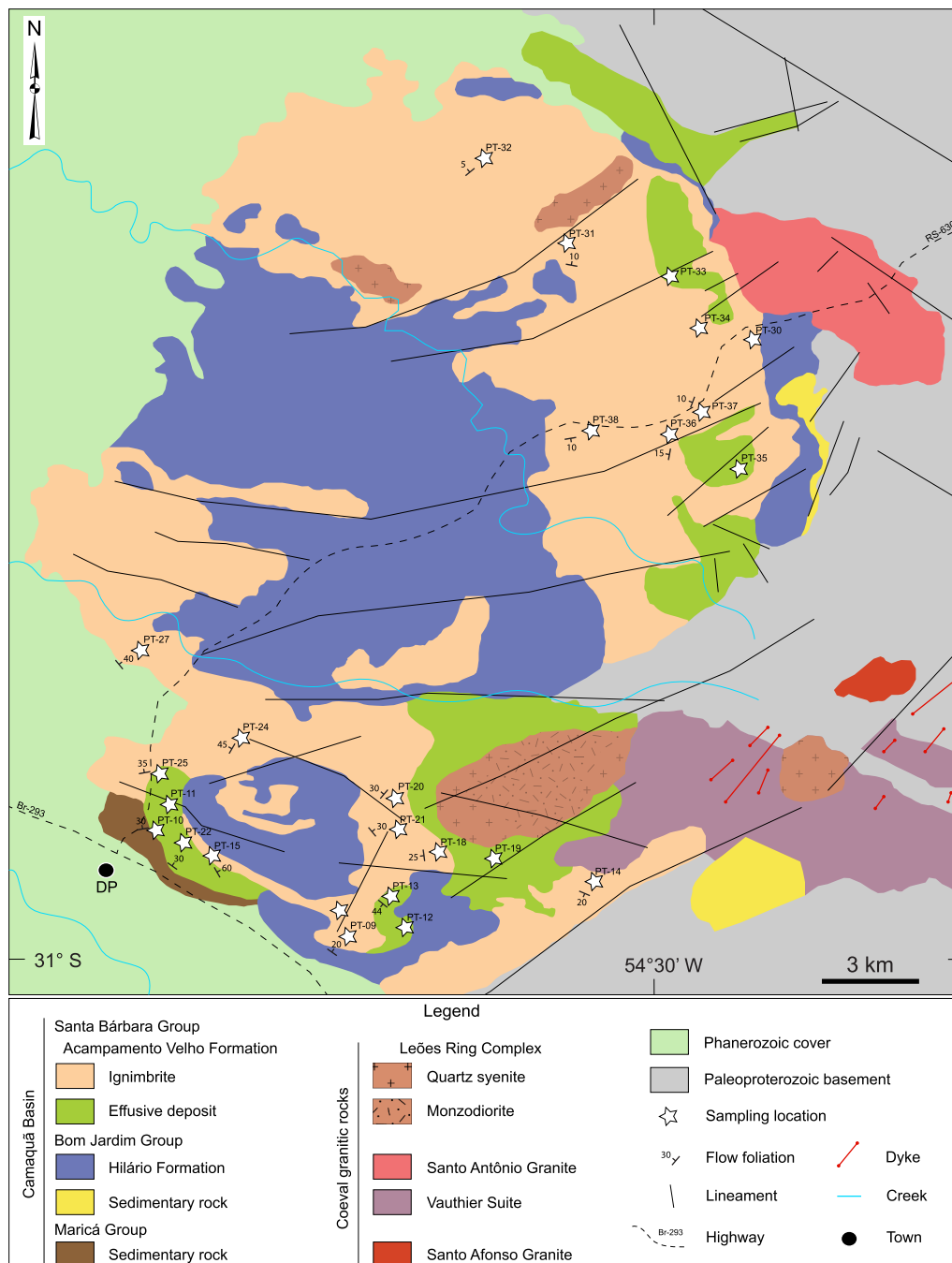


Fig. 2. Geological map of the Taquarembó Plateau (modified from Gastal, 1999; Sommer et al., 1999). Flow foliation from sites is on the figure.

stratigraphic units (Paim et al., 2000, 2014).

The magmatism of the CB is characterized by three volcanic cycles that evolved from calc-alkaline high-K and shoshonitic (Hilário volcanism) to sodic alkaline (Acampamento Velho volcanism) and finally to transitional and tholeiitic magmas (Rodeio Velho volcanism). The crustal contribution is represented by peraluminous granitoids (Fig. 1) (Wildner et al., 2002; Sommer et al., 2006; Lima et al., 2007).

The volcanism associated to the Acampamento Velho Formation is characterized predominantly by felsic sodic-alkaline magmatism (Sommer et al., 2013) of Ediacaran age (574 – 549 Ma) (Sommer et al., 1999, 2005, 2006; Chemale, 2000; Janikian et al., 2008; Matté et al., 2016). This magmatism generated significant volcanic deposits (Fig. 1), where the successive pulses were responsible for the formation of volcanic plateaus (Taquarembó Plateau and Ramada Plateau; Sommer et al., 1999). Ignimbrites with different types of deposits were predominantly characterized by rhyolitic explosive eruptions. Rhyolite flows and sin-volcanic intrusives represented effusive eruptions. Basic effusive deposits occur locally, mainly in the final stages of volcanism.

2.1. Geology of Taquarembó Plateau

The Taquarembó Plateau (TP) is a geomorphological feature with 32 km (N-S) × 25 km (E-W) and an average thickness of 150 m. The TP is localized close to the Dom Pedrito town in south Brazil (Fig. 1).

The plateau is constituted mainly by volcanic deposits correlated to Hilário and Acampamento Velho Formations (Sommer et al., 1999). Hilário Formation rocks occur at the base of the plateau and are characterized by basic-intermediate lava flows and sin-volcanic intrusives, besides of volcanogenic sedimentary deposits. The Acampamento Velho Formation deposits are the most abundant and are represented in the basal portions mainly by pyroclastic deposits followed by effusive silicic rocks (AVF; Fig. 2) (Sommer et al., 1999, 2013).

Ignimbrites are the predominant pyroclastic deposits. Facies distribution is variable, but lapillistone and lapilli-tuffs are dominant, ranging from stratified and partially welded deposits to massive ignimbrites with a high degree of welding (rheoignimbrites). The main constituents are the juvenile fragments such as crystal fragments of quartz and K-feldspar, pumices and shards. At the basal portion of the deposits, cognate lithic fragments are more abundant than accidental and accessories fragments originated from the country rocks.

The effusive deposits are characterized predominantly by lava flows and synvolcanic bodies. Rhyolite lava flows facies vary between auto-brecciated, foliated and massive portions (Sommer et al., 1999, 2005, 2006, 2011, 2013; Lima et al., 2007) with aphanitic texture. Synvolcanic bodies are represented mainly by massive porphyritic trachytes and rhyolites characterized by K-feldspar phenocrysts set in an aphanitic matrix.

In the southeastern border of this plateau occurs an intrusive complex (Leões Ring Complex - LRC), with approximately 5 × 4 km (Gastal 1999) characterized by an association of monzodiorites to quartz-monzodiorites in the central part, surrounded by quartz-syenites (Fig. 2) (Sommer et al., 1999; Gastal, 1999). The rocks present an alkaline affinity and age of 572 ± 3 Ma (Gastal and Lafon, 2001). The relationship between these intrusives and the volcanic sequence is still unclear. Previous work based on field and geochemical data (Sommer et al. 1999) suggests the intrusive complex can represent the intrusive portion of a caldera structure, whose collapse may have generated part of the acid volcanism of the TP.

3. Material and methods

3.1. Fieldwork

The fieldwork involved detailed geological mapping, and structural measurements performed with a magnetic compass and GPS receptor. The field data was processed and compiled using ArcMap 10.5 (ESRI),

while the structural data was analyzed using contour plots processed in Stereonet 10. The fieldwork also included sampling for petrography and magnetic anisotropy (AMS and AARM).

3.2. Magnetic mineralogy characterization

In AMS and AARM studies for the determination of flow directions of lavas and pyroclastic deposits, it is essential to identify the mineral phases that contribute to the magnetic susceptibility and the magnetic remanence of the rocks and their anisotropy (e.g., Rochette et al., 1999; Magee et al., 2016; Moncinhatto et al., 2020; Pasqualon et al., 2020). Rock magnetic experiments were performed in samples from all sampling sites, to improve the interpretation of AMS and AARM data. All magnetic measurements were processed at the Laboratório de Paleomagnetismo of Universidade de São Paulo (USPMag), São Paulo, Brazil.

Isothermal remanent magnetization (IRM) acquisition, hysteresis loops and backfield curves were performed for the characterization of the ferromagnetic phases and their magnetic properties. From these measurements we obtained the saturation magnetization (M_s), saturation remanent magnetization (M_{rs}), coercivity (H_c) and coercivity of remanence (H_{cr}) (e.g., Dunlop and Özdemir, 1997). All sampled sites were measured, processed on the MicroMag 3900 vibrating sample magnetometer (VSM, Princeton Measurement Corporation) with a maximum inducing field of 1 T. In order to characterize the domain structure of ferromagnetic phases and to identify and discriminate the different magnetic mineral assemblages, we used first-order reversal curves (FORCs; Roberts et al., 2000, 2014). This method allows differentiating single domain (SD), multidomain (MD) and pseudo-single domain (PSD) or vortex structures. FORC diagrams were obtained for nine sites on the same VSM, at room temperature after 200 reversal curves, with an averaging time of 200 ms. FORC diagrams were generated using the FORCinel software (Harrison and Feinberg 2008) with a smoothing factor of 5.

The measurements of magnetic susceptibility versus temperature were obtained to determine the Curie or Néel temperatures of magnetic minerals (e.g., Dunlop and Özdemir, 1997). High-temperature curves were performed between 30 and 700 °C. Magnetic susceptibility was measured every 8.6 °C with the Kappabridge KLY-4S susceptometer coupled with a CS3 furnace (Agico Ltd.) for 27 sampling sites. After measurements, the raw data were corrected with the software Cureval8 (Agico Ltd.) for the susceptibility of the empty sample holder. Transition temperatures of magnetic minerals (Curie temperatures, T_c) were obtained by the Petrovský and Kapička (2006) method, based on the beginning of the paramagnetic hyperbola at the T_c .

3.3. Sampling methods and AMS measurements

The AMS analyses were performed at 32 sites, 22 for ignimbritic deposits and 10 for effusive deposits. For each site, 7–10 oriented cores were collected using a portable gasoline-powered drill with a non-magnetic diamond-tipped drill bit. At the laboratory, the cores were cut into standard specimens, 2.5 cm in diameter and 2.2 cm in height, using a diamond-tipped, non-magnetic saw blade, totalizing 377 standard specimens (250 for ignimbrites and 127 for effusive deposits). All measurements were made at the USPMag, on a Kappabridge MFK1-FA susceptometer (Agico Ltd.) operating at room temperature and at a field of 200 A/m and 976 Hz of frequency, with a sensitivity of about 2×10^{-8} SI. Directional data and scalar parameters were processed using the Anisoft 5 software (Agico Ltd.). The bootstrap statistical analysis tool of Tauxe et al. (1991) and the Jelínek (1978) statistics were used to evaluate the magnetic tensors and interpret the flow patterns of volcanic deposits. The AMS directional data from individual sites were filtered to eliminate sites with high internal dispersion (E_{1-2} , E_{2-3}), removing sites with uncertainty estimates $>26.5^\circ$ following the criterium of Jelínek (1978).

The AMS provides information on the petrofabrics of rocks through

the preferred orientation of their magnetic minerals. The technique consists of measuring the magnetic susceptibility for each specimen in different directions, obtaining magnetic susceptibility tensor (Tarling and Hrouda, 1993). The magnitude (eigenvalues) and orientation (eigenvectors) of the maximum (K_1), intermediate (K_2) and minimum (K_3) principal axes of susceptibility ($K_1 \geq K_2 \geq K_3$) are represented by a magnetic anisotropy ellipsoid (Tarling and Hrouda, 1993). The K_1 axis defines the magnetic lineation (L), while the K_3 axis is the pole of the magnetic foliation (F), marked by the plan between K_1 and K_2 . The mean magnetic susceptibility (Km) is calculated by the arithmetical mean of the three main axes of susceptibility ($Km = [K_1 + K_2 + K_3]/3$). Jelinek (1981) described the shape parameter of the magnetic susceptibility ellipsoid, expressed by $T = (\ln F - \ln L)/(\ln F + \ln L)$, where $F = K_2/K_3$ (planar anisotropy) and $L = K_1/K_2$ (linear anisotropy). The shape parameter varies from $T = +1$ for a pure oblate ellipsoid to $T = -1$ for a pure prolate ellipsoid; $T = 0$ for a triaxial ellipsoid. The method also allows quantifying the degree of anisotropy, defined by $P = K_1/K_3$.

3.4. Anisotropy of anhysteretic remanent magnetization (AARM) measurements

The AARM was used to isolate the contribution of remanence-bearing minerals from that of paramagnetic and/or diamagnetic matrix (Jackson 1991). AARM is acquired after simultaneously submitting the sample to an alternating magnetic field (AF) and a small bias field. These steps are performed along different directions of the sample. Here we used the 12-position scheme, which provided reliable results for ignimbritic rocks in a previous study (Moncinhatto et al., 2020). The AARM tensor is represented similarly to the AMS, being expressed by the magnitude (eigenvalues) and orientation (eigenvectors) of the maximum (M_1), intermediate (M_2) and minimum (M_3) principal axes of anhysteretic remanence ellipsoid (Jackson 1991). The advantage of this method is that it excludes the SD effect of magnetites that generate inverse AMS fabric (Stephenson et al., 1986), improving the interpretation of directional data for volcanic deposits. The AARM acquisitions were performed with an LDA3-AMU1 (Agico Ltd.) to demagnetize/magnetize the samples and with a JR6A magnetometer (Agico Ltd.) for subsequent remanence measurements, applying an AF peak field of 100 mT and a bias field of 0.5 mT for each specimen (6 per site).

4. Results

4.1. Field observations

Pyroclastic and effusive deposits have been described on the Taquarembó Plateau in previous works with a petrological and volcanological focus (e.g. Sommer et al., 1999, 2011, 2013; Wildner et al., 1999). Here we described five main lithofacies (Table 1). Based on their main textural characteristics, for this study, ignimbrites were grouped into stratified ignimbrites and rheomorphic ignimbrites whose contact between these deposits is marked by an erosive discordance (Sommer et al., 2013) (Fig. 3b).

Table 1

Terminology adopted for ignimbritic deposits of the Acampamento Velho volcanism in the Taquarembó Plateau (modified from Sommer et al., 2013).

Unit	Facies code	Lithofacies description
Rheomorphic	rheoLT	Massive and poorly sorted lapilli-tuff with a strongly flattened and stretched vitriclastic matrix; parataxitic texture
Stratified	LT(nl-ip)	Poorly sorted lapilli-tuff with normal grading of lithic fragments and reverse grading of pumice
	llT	Lithic-rich lapilli-tuff
	eLT	Lapilli-tuff with eutaxitic texture
	crLT	Crystal-rich lapilli-tuff

Stratified ignimbrites are deposits of tabular geometry arranged in subhorizontal layers (Fig. 3b), poorly sorted, generally presenting normal grading pattern of lithic fragments (ranging from 1 to 6 cm of rhyolitic and andesitic composition) and an increase of pumice fragments to the top (reverse grading). Stratified ignimbrites facies vary from lapilli-tuffs rich in lithic fragments and crystals (Fig. 3f) to lapilli-tuffs with eutaxitic texture (Fig. 3e) present in practically the whole layer, tending to parataxitic at the top of each deposit. Some facies present levels rich in blocks and bombs size fragments (Fig. 3d), occurring mainly at the top. Fractures and cavities filled with quartz were also observed in several portions, indicating an increase in volatile content with probable gas escape.

Rheomorphic ignimbrites occur in the upper portion of the ignimbrites sequence (Fig. 3a). They show little variation throughout the deposits compared to the stratified ignimbrites, being predominantly homogeneous with porphyritic aspect and associated rheomorphism (Fig. 3c). Rheomorphic ignimbrites display strong flattening of glass shards and pumices, characterized by parataxitic texture, indicating a high degree of welding (Sommer et al., 2013). In general, it is a poorly sorted rock with a higher occurrence of lithic fragments at the base and crystals fragments dispersed in an ash-sized matrix at the top.

The effusive deposits are locally distributed in the TP, mainly as lava flows and also as structures that resemble domes. Dikes and sills occur too (Fig. 2). Some outcrops showed trachytic lava flows interbedded with pyroclastic deposits (Fig. 3a). Effusive deposits are represented by trachytes and rhyolites with porphyritic texture, characterized by euhedral quartz and K-feldspar phenocrystals (<10%) dispersed in an aphanitic matrix. There was an increase in the number of vesicles filled with carbonate and silica towards the top of the deposits, indicating that the deposits interspersed with the ignimbrites are lava flows.

In order to assist AMS analysis, structural data were collected for most AMS sampling sites (Fig. 2). The rheomorphic ignimbrites are marked by flow foliations with a higher dip (>20°) compared to stratified ignimbrites (<20°) and similarly to the effusive deposits. Imbricated logs such as the orientation of flattened pumices are the main features of flow foliation, evidenced by the strong eutaxitic texture, tending to parataxitic in deposits with a high degree of welding.

4.2. Magnetic mineralogy

The analysis of IRM acquisition curves, hysteresis loops (Table 2) and FORC diagrams demonstrated four distinct behaviours for the studied samples (Fig. 4). The first behaviour is marked by the non-saturation of IRM curves up to 1 T, showing inflections at fields around 100 mT and 500 mT (Fig. 4a). Hysteresis loops exhibit coercivities < 100 mT (Fig. 4b) and a wasp-waisted shape (Roberts et al., 1995; Tauxe et al., 1996) indicating ferromagnetic phases of different coercivities. FORC diagrams are typical of SD grains (Fig. 4c), which are characterized by closed concentric contours around the central peak at 30 mT and a sharp horizontal ridge at $B_u = 0$ (e.g., Roberts et al., 2014, 2018). This behaviour is observed on sites PT-02, PT-12 (effusive rocks), PT-03, PT-06, PT-07, PT-08 and PT-36 (pyroclastic rocks). The second behaviour is characterized by IRM acquisition curves that still not saturated at the maximum applied field of 1 T (Fig. 4d), suggesting the dominance of high-coercivity minerals (e.g., hematite). However, the hysteresis loops show strong coercivities and are goose-necked (Fig. 4e) suggesting the coexistence of low-coercivity (e.g., magnetite) phases with higher amounts of high-coercivity (e.g. hematite) phases (Roberts et al., 1995; Tauxe et al., 1996). FORC diagrams (Fig. 4f) are typical of MD grains. This second behaviour is identified on sites PT-01, PT-05, PT-09, PT-15, PT-18, PT-21, PT-30 (pyroclastic rocks), PT-10, PT-13, PT-19 and PT-33 (effusive rocks). The third behaviour shows IRM acquisition curves fully saturated at 1 T (Fig. 4g). The acquisition curves of these samples typically exhibit a rapid increase and reach >90% saturation below 200 mT (Fig. 4g), implying a high concentration of low-coercivity magnetic carriers in these specimens. Hysteresis loops are narrow-waisted

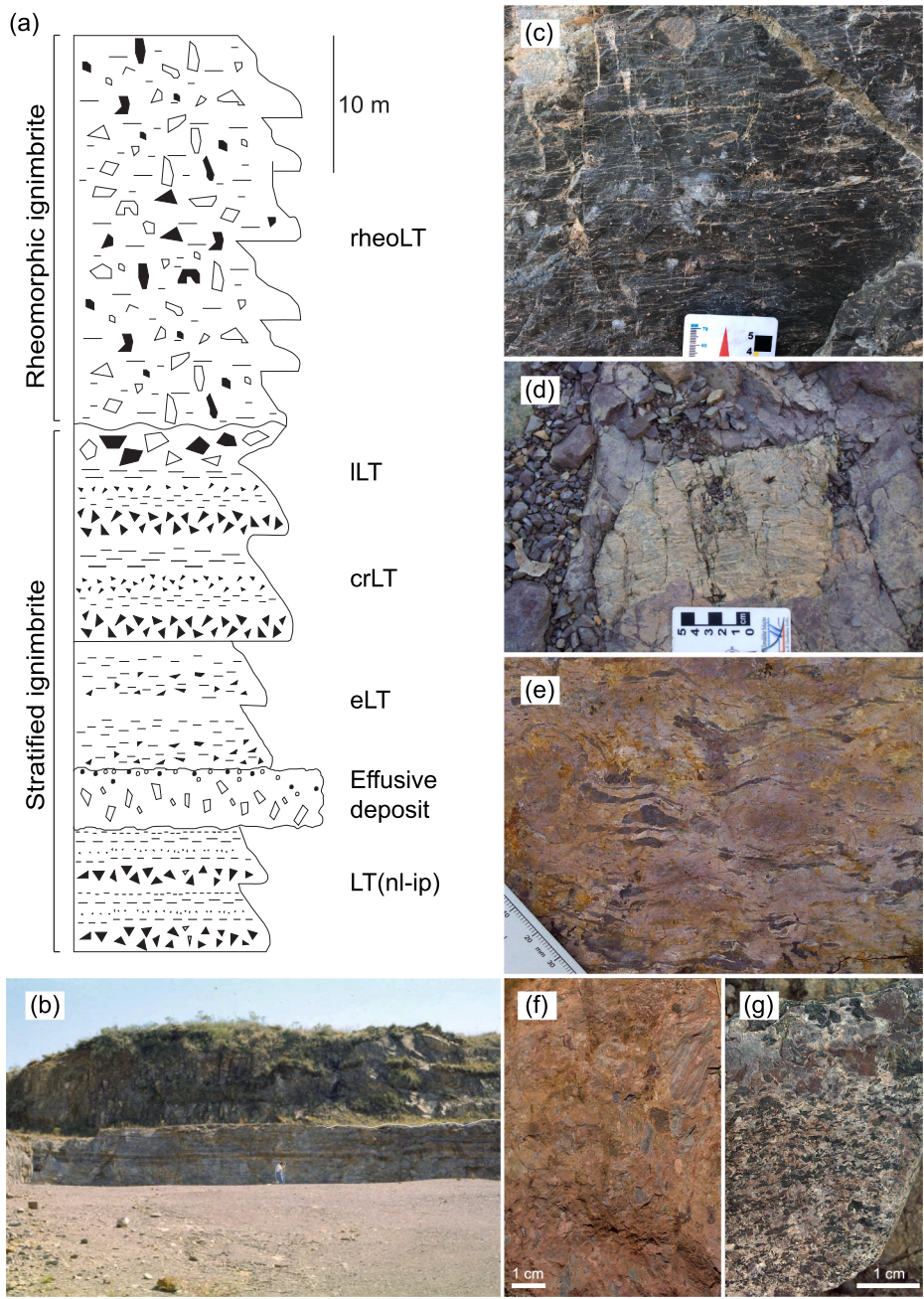


Fig. 3. Schematic columnar profile (a) of the ignimbritic deposits of the Taquarembó Plateau with their respective facies code (the description is displayed in Table 1). The contact between rheomorphic and stratified ignimbrites is marked by the white line (b). (c) Parataxitic texture related to the rheomorphic ignimbrites (rheoLT). (d and f) Lappiltuff rich in lithic fragment (ILT). (e) Eutaxitic texture in welded stratified ignimbrites (eLT). (g) Pumice, crystal and lithic fragments related to stratified deposits (LT-nl-ip).

(Fig. 4h), corroborating the dominance of low-coercivity phases. FORC diagrams (Fig. 4i) exhibit closed contours centred around $B_c = 25$ mT. Also, there is a broad vertical distribution of B_u along the $B_c = 0$ line, mostly within the range of around 40 mT. These features are typical of magnetite with magnetic vortex state or mixtures of SD and MD magnetite grains (Roberts et al., 2018). This behaviour comprises PT-04, PT-20, PT-24, PT-37 (pyroclastic rocks) and PT-35 (effusive rocks). The fourth behaviour does not saturate at 1 T, but shows a very narrow waist in the hysteresis loops which have a wasp-waisted shape. The FORC diagram (Fig. 4f) indicates MD grains. This pattern is observed on PT-14, PT-27, PT-31, PT-32, PT-34, PT-38 (pyroclastic rocks), PT-11, PT-22 and PT-25 (effusive rocks).

The Curie temperature (T_c) of samples provides important evidence for identifying the magnetic mineralogy (Dunlop and Özdemir, 1997). Representative thermomagnetic curves of ignimbrite and effusive deposits (Fig. 5) show two significant drops in susceptibility at Curie

temperatures near 580 °C (magnetite) and 675 °C (hematite). These results corroborate the IRM and hysteresis curves that show a mixture of magnetic minerals for most sampled sites. Except for the site PT-20, which shows reversible behaviour, all rocks suffer considerable mineralogical transformation during heating. The heating curves of the Fig. 5a and 5b show a steep fall at a temperature of approximately 580 °C, suggesting that Ti-poor magnetite and/or magnetite is the main ferromagnetic carrier. Besides, hematite/titanohematite is present in this sample and can be identified because the magnetic susceptibility only dies out completely after 580 °C. A sharp Hopkinson peak was observed in Fig. 5b, generating a good estimative for T_c (Petrovský and Kapička, 2006). Samples from ignimbrites show reversible curves during heating-cooling cycles (Fig. 5c) and magnetic susceptibility with a high-temperature transition at 580–590 °C, suggesting the presence of magnetite or titanomagnetite with low Ti content. A significant decrease in susceptibility between 300 and 350 °C was found in sample PT-27

Table 2

Measured hysteresis parameters for studied sites. M_s = saturation magnetization; M_{rs} = saturation remanent magnetization; H_c = coercivity; H_{cr} = remanent coercivity. Not read hysteresis parameters as (-).

Lithology	Site	UTM coord.		M_s (Am ² /kg)	M_{rs} (Am ² /kg)	H_c (mT)	H_{cr} (mT)	H_{cr}/H_c	M_{rs}/M_s	
		mE	mN							
Ignimbrites	PT-01	759,483	6,569,331	1.77E-02	4.93E-03	4.77E-02	7.74E-02	8.36E + 00	2.79E-01	
	PT-03	729,750	6,569,228	1.15E-02	5.71E-03	1.20E-01	3.47E-01	2.90E + 00	4.95E-01	
	PT-04	729,813	6,569,351	3.27E-02	8.71E-03	1.75E-02	4.65E-02	2.65E + 00	2.67E-01	
	PT-05	729,826	6,569,357	8.56E-03	4.85E-03	1.80E-01	3.93E-01	2.18E + 00	5.66E-01	
	PT-06	729,506	6,569,415	8.13E-03	4.95E-03	2.55E-01	5.11E-01	2.01E + 00	6.08E-01	
	PT-07	729,503	6,569,517	7.51E-03	5.35E-03	3.78E-01	5.11E-01	1.35E + 00	7.12E-01	
	PT-08	729,586	6,569,463	1.18E-02	2.95E-03	1.66E-02	4.37E-01	2.62E + 01	2.49E-01	
	PT-09	729,810	6,568,732	9.11E-03	6.46E-03	2.73E-01	4.06E-01	1.49E + 00	7.10E-01	
	PT-14	737,063	6,570,415	5.44E-06	8.68E-07	1.81E-01	-	-	1.59E-01	
	PT-15	725,463	6,571,988	1.67E-06	8.98E-07	1.74E-01	-	-	5.38E-01	
	PT-18	732,484	6,571,513	1.72E-06	5.14E-07	4.49E-02	-	-	2.99E-01	
	PT-20	731,236	6,573,132	6.95E-05	1.04E-05	1.56E-02	-	-	1.49E-01	
	PT-21	731,331	6,572,311	1.73E-06	4.99E-07	4.10E-02	-	-	2.88E-01	
	PT-24	726,848	6,575,495	5.96E-07	2.57E-07	6.42E-02	-	-	4.32E-01	
	PT-27	723,960	6,578,532	4.06E-06	6.95E-07	1.86E-02	-	-	1.71E-01	
	PT-30	742,131	6,588,694	3.94E-07	1.91E-07	1.56E-01	-	-	4.86E-01	
	PT-31	736,729	6,592,109	3.27E-05	4.19E-06	1.22E-02	-	-	1.28E-01	
	PT-32	734,373	6,595,060	3.68E-05	6.69E-06	1.72E-02	-	-	1.82E-01	
	PT-34	740,567	6,589,117	7.37E-06	9.77E-07	1.27E-02	-	-	1.33E-01	
	PT-36	739,603	6,585,486	1.77E-06	5.94E-07	6.21E-02	-	-	3.35E-01	
	PT-37	740,545	6,586,260	1.85E-06	6.32E-07	6.52E-02	-	-	3.41E-01	
	PT-38	737,321	6,585,654	1.84E-06	2.00E-07	1.25E-02	-	-	1.09E-01	
	Lavás	PT-02	759,530	6,569,327	2.92E-02	9.71E-03	4.53E-02	2.03E-01	4.47E + 00	3.33E-01
		PT-10	724,212	6,572,560	6.19E-03	2.81E-03	1.12E-01	3.23E-01	2.89E + 00	4.54E-01
		PT-11	724,541	6,573,017	4.44E-01	1.39E-01	4.04E-02	8.91E-02	2.21E + 00	3.13E-01
		PT-12	731,426	6,568,949	6.38E-06	2.10E-06	6.54E-02	-	-	3.30E-01
		PT-13	730,962	6,570,110	7.32E-07	5.32E-07	4.22E-01	-	-	7.27E-01
		PT-19	734,116	6,571,218	2.91E-06	1.21E-06	7.95E-02	-	-	4.17E-01
		PT-22	724,926	6,572,450	8.69E-05	1.21E-05	1.92E-02	-	-	1.39E-01
		PT-25	724,457	6,574,354	1.92E-05	3.79E-06	2.06E-02	-	-	1.98E-01
		PT-33	739,670	6,590,862	1.46E-06	7.78E-07	1.71E-01	-	-	5.32E-01
		PT-35	741,569	6,584,241	4.73E-05	8.50E-06	1.89E-02	-	-	1.80E-01

(Fig. 5d), possibly corresponding to T_c of maghemite (e.g., Deng et al., 2001; Dedzo et al., 2011). Subsequently, there is a substantial decrease in magnetic susceptibility within the interval of 575–585 °C, demonstrating the presence of magnetite.

4.3. AMS data

4.3.1. Scalar results

The mean values of the degree of anisotropy (P), shape parameter (T), magnetic susceptibility (Km), lineation (L) and foliation (F) for each paleomagnetic site are presented in Table 3. Pyroclastic deposits were separated into rheomorphic and stratified ignimbrites due to the difference shown in the $P \times Km$ graph (Fig. 6a). Magnetic susceptibility values range from 0.04 to 6.30×10^{-3} SI for stratified ignimbrites, 0.05 to 3.91×10^{-3} SI for rheomorphic ignimbrites and 0.06 to 9.71×10^{-3} SI for effusive deposits. Effusive deposits and stratified ignimbrites present higher susceptibility ($>0.5 \times 10^{-3}$ SI) compared to rheomorphic ignimbrites ($<0.5 \times 10^{-3}$ SI). The difference in susceptibility can be explained due to the variation in the amount and types of magnetic mineral content (Moncinhatto et al., 2020), where susceptibility values $> 0.5 \times 10^{-3}$ SI can be related to a predominant ferromagnetic behaviour of the studied deposits (e.g., Tarling and Hrouda, 1993).

The degree of anisotropy for each site varies from 1 to 11% (average of 3.75%) for ignimbrites and 0.4 to 3.5% (average of 1.68%) for effusive deposits. These values are considered typical for pyroclastic flow deposits and trachytic-rhyolitic lava flows (e.g. Tarling and Hrouda, 1993; Giordano et al., 2008; Agrò et al., 2015). No correlation can be inferred between magnetic susceptibility and the anisotropy percentage (Fig. 6a), nonetheless samples with higher P show low Km values for both deposits.

Regarding the shape of the anisotropy ellipsoid, there is a greater tendency for planar anisotropy (vary from 0.5 to 7.5%) than linear (vary

from 0.3 to 3.6%) for ignimbritic deposits, whereas effusive deposits present similar L and F values ($L = 0.1 - 1.4\%$; $F = 0.2 - 2\%$). From the 377 samples, 220 present an oblate shape (87 with $T > 0.5$) and 157 a prolate shape (41 with $T < -0.5$) as shown in Fig. 6b. There is a direct correlation between the increase in the degree of anisotropy and the magnetic foliation (Fig. 6c). Corroborating with this, the sites that presented higher P and F are also those that exhibited higher values of T (oblate ellipsoid), indicating a dominant planar magnetic fabric.

4.3.2. Directional data

The mean AMS eigenvectors and the 95% confidence ellipses ($E_{1,2}$ and $E_{1,3}$) for each site are presented in Table 3. The AMS directional data (Fig. 7) were interpreted based on the distribution of the magnetic axes (K_1 , K_2 and K_3) at the equal-area stereographic projection and their confidence zones (Jelinek, 1978), allowing the classification of the magnetic fabrics for the studied volcanic deposits. Sites PT-13 and PT-30 were filtered from the directional interpretation due to their high internal dispersion ($E_{1,2}$, $E_{2,3} > 26.5^\circ$). In the pyroclastic deposits, three magnetic fabrics were defined for both ignimbrites facies according to the eigenvectors orientations. These fabrics types are known as normal, intermediate and inverse, whose classifications are widely discussed in several papers (e.g., Le Pennec et al., 1998; Rochette et al., 1999; Giordano et al., 2008; Pueyo Anchuela et al., 2014; Agrò et al., 2015).

In this work, we group the three types of AMS fabric for ignimbrites proposed by Agrò et al. (2015) as a sub-division of the normal fabric, which are: (i) parallel, when the magnetic foliation ($K_1 - K_2$ plane) is gently imbricated and K_1 is close to the foliation plunge (Fig. 8a and 8b). This fabric is observed in 4 sites (Figs. 7 and 10b; PT-05, 15, 31 and 34). (ii) Transverse, when the K_1 is orthogonal to the foliation plunge (Fig. 8c and d), identified on 6 sites (Figs. 7 and 10b; PT-01, 09, 14, 21, 27 and 32). (iii) Oblique, when the K_1 is oblique (between 35° and 55°) with the foliation plunge (Fig. 8e and 8f). This behaviour is observed in 2 sites

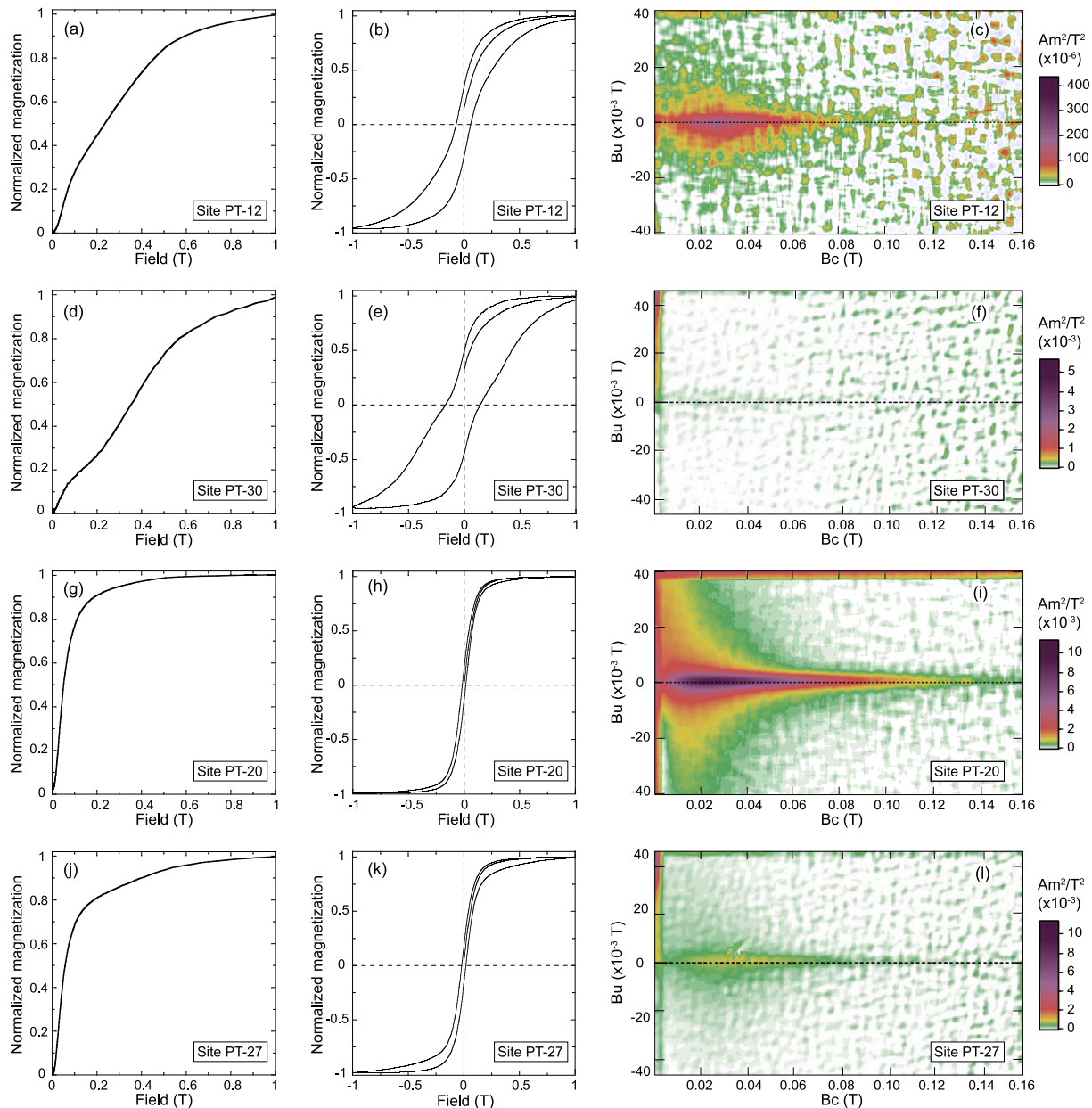


Fig. 4. IRM acquisition curves (a, d, g and j), hysteresis loops (b, e, h and k) and FORC diagrams (c, f, i and l) for the studied volcanic rocks of Taquarembó Plateau (sites PT-12, PT-20, PT-27 and PT-30).

(Fig. 7; PT-18 and 38). In all fabric types, the K_3 is nearly vertical, being the most reliable axes to infer flow direction, based on the imbricated pattern of magnetic foliations (Dedzo et al., 2011).

The interchange of K_1 and K_3 axes characterizes the inverse fabric type (e.g. Rochette et al., 1999; Agrò et al., 2015; Moncinhatto et al., 2020). This inverse pattern is attributed to small SD grains of magnetite that have K_1 perpendicular to the long axis of the crystal, generating an exchange of K_1 and K_3 AMS axes (Potter and Stephenson 1988). This fabric is observed in 6 sites (Figs. 7 and 10b; PT-03, 04, 06, 07, 08 and 36). Intermediate AMS fabric occurs when the K_2 axis is sub-vertical. This behaviour is observed in 3 sites (Fig. 7; PT-20, 24 and 37).

Directional data for effusive deposits show quite similar behaviour of magnetic axes with the ignimbrites. Normal fabric is identified in 6 sites (Fig. 7; PT-10, 11, 19, 22, 25 and 33) and inverse in 3 sites (Figs. 7 and 10b; PT-02, 12 and 35) for lavas, based on the classification proposed by Rochette et al. (1992). The inverse fabric of effusive deposits is similar to the ignimbrites. However, the plan between K_2 and K_3 is much more

evident in the AMS stereograms of lavas.

4.4. AARM × AMS data

The AARM data were used to prove the inverse and intermediate fabrics for the studied volcanic rocks. Inverse fabric occurs at sites that showed magnetites with FORC diagrams typical of SD grains (e.g., Fig. 4c), while the intermediate at sites with FORC diagrams presenting vortex structure or mixtures of SD and MD magnetite grains (Fig. 4i). The interpretation of the AARM and AMS tensors (Fig. 9) for the same samples allows identifying an interchange between the K_2 and K_3 axes for the intermediate fabric (Fig. 9a and 9c) and between K_1 and K_3 in inverse fabric (Fig. 9b and 9d). Besides, AMS data that show an intermediate fabric also present the K_2 sub-vertical and a well-defined K_2 - K_3 plane (Fig. 9a). For the inverse fabric, the K_1 axis is sub-vertical in the AMS stereogram (Fig. 9b) being thus normal to the bedding plane observed in the field.

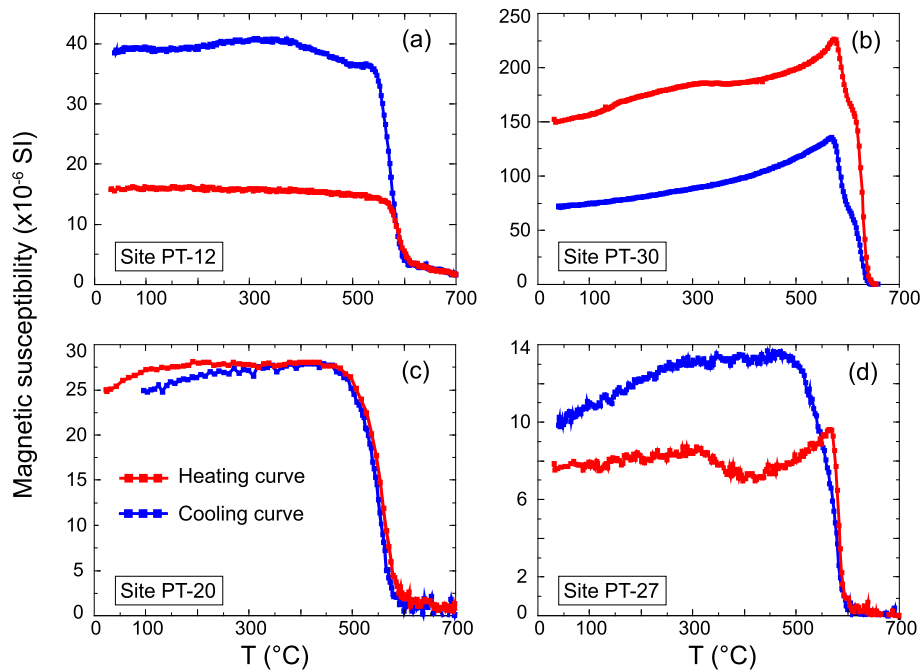


Fig. 5. Representative thermomagnetic curves of the magnetic mineralogy of volcanic deposits from Taquarembó Plateau. Heating curve (red) and cooling curve (blue) were obtained between room temperature and 700 °C.

Table 3

AMS results for the studied sites. n = number of specimens measured; K_m = mean magnetic susceptibility; L = magnetic lineation; F = magnetic foliation; P = degree of anisotropy; T = shape parameter; D = declination; I = inclination; $E_{1,2}$ and $E_{1,3}$ = semi-angles of the 95 per cent confidence ellipses around the susceptibility axes.

Lithology	Site	n	Scalar results				Directional results				
			$K_m(10^{-3}SI)$	L	F	P	T	$K_1(D/I)$	$K_3(D/I)$	$E_{1,2}$	$E_{1,3}$
Ignimbrites	PT-01	13	0.732	1.027	1.054	1.083	0.252	347/15	221/65	011/05	024/05
	PT-03	13	1.35	1.020	1.021	1.041	-0.011	075/76	220/11	022/13	020/05
	PT-04	12	1.35	1.015	1.023	1.038	-0.002	326/50	063/06	022/18	045/20
	PT-05	7	0.08	1.016	1.029	1.046	0.484	013/58	211/31	020/12	031/15
	PT-06	8	0.149	1.023	1.056	1.080	0.174	301/38	199/15	031/29	067/07
	PT-07	7	0.05	1.032	1.075	1.109	0.436	357/05	094/53	035/06	035/07
	PT-08	9	0.597	1.016	1.043	1.060	0.461	331/80	065/01	027/03	006/04
	PT-09	7	0.07	1.031	1.049	1.081	0.395	164/12	042/68	020/14	021/12
	PT-14	13	0.648	1.010	1.010	1.020	0.028	295/02	029/57	012/07	022/07
	PT-15	13	0.11	1.011	1.009	1.021	-0.178	242/18	049/72	025/10	019/13
	PT-18	10	0.194	1.008	1.010	1.018	0.310	274/26	043/52	036/03	027/04
	PT-20	8	3.91	1.036	1.010	1.046	-0.444	103/12	289/78	014/04	024/12
	PT-21	9	0.239	1.004	1.006	1.010	0.246	180/12	282/42	048/23	049/07
	PT-24	11	0.08	1.005	1.004	1.010	-0.113	132/21	332/67	018/10	021/10
	PT-27	15	0.755	1.031	1.014	1.045	-0.346	220/13	111/54	005/03	008/05
	PT-30	26	0.04	1.006	1.005	1.011	0.074	104/34	300/55	040/32	039/32
	PT-31	15	6.9	1.005	1.007	1.012	0.237	247/10	045/79	014/11	012/09
	PT-32	9	5.06	1.013	1.012	1.025	-0.012	273/04	161/80	030/07	014/07
	PT-34	14	0.923	1.003	1.012	1.016	0.405	101/04	262/85	046/07	010/09
	PT-36	8	0.406	1.008	1.011	1.019	0.282	168/79	330/11	020/05	018/05
PT-37	13	0.208	1.005	1.005	1.010	0.070	055/08	148/20	013/04	026/10	
PT-38	10	0.563	1.007	1.015	1.022	0.417	224/06	121/65	024/10	014/08	
Lavás	PT-02	15	0.69	1.006	1.008	1.014	0.126	254/52	017/23	023/11	058/12
	PT-10	12	0.17	1.014	1.020	1.034	0.305	238/31	332/06	051/37	052/17
	PT-11	7	9.71	1.004	1.004	1.008	-0.082	185/65	315/16	031/15	027/16
	PT-12	17	0.486	1.009	1.002	1.011	-0.460	052/78	151/02	006/04	015/04
	PT-13	13	0.06	1.015	1.013	1.028	0.058	243/04	334/65	038/18	057/31
	PT-19	14	0.261	1.001	1.002	1.004	0.182	074/47	262/42	040/22	032/06
	PT-22	13	9.63	1.006	1.018	1.024	0.543	149/05	252/70	024/14	022/13
	PT-25	13	3.29	1.010	1.009	1.019	-0.071	190/25	056/56	009/04	014/05
	PT-33	9	0.08	1.007	1.009	1.016	0.181	322/13	065/44	046/15	026/20
	PT-35	14	8.69	1.008	1.008	1.016	0.051	112/59	356/15	011/04	029/05

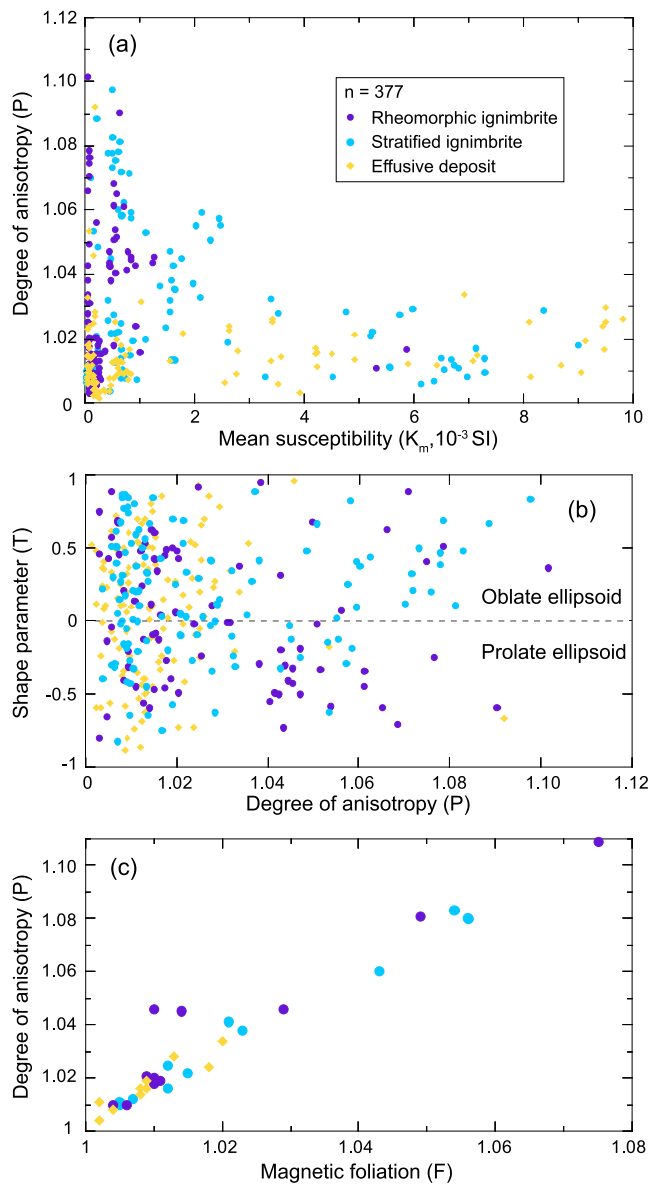


Fig. 6. Scalar results of AMS analyses: (a) degree of anisotropy (P) versus mean magnetic susceptibility (K_m) for all specimens; (b) shape parameter (T) versus degree of anisotropy (P) plot for all specimens; (c) degree of anisotropy (P) versus magnetic foliation (F) for mean value of each site displayed in Table 3.

5. Discussion

5.1. Relationship between magnetic mineralogy and fabric patterns

A detailed study of the magnetic mineralogy and a good geological field control are essential when using the AMS data for the interpretation of flow directions of volcanic deposits (e.g., Stephenson et al., 1986; Borradaile, 1987; Potter and Stephenson, 1988; Cañón-Tapia, 2004; Chadima et al., 2009; Cañón-Tapia and Mendoza-Borunda, 2014; Magee et al., 2016; Wiegand et al., 2017; Moncinhatto et al., 2020; Pasqualon et al., 2020). Standard rock magnetic analyses indicate magnetite or Ti-poor magnetite as the main magnetic carrier for ignimbrites and effusive deposits in the TP. AMS sites that present MD grains exhibit a normal magnetic fabric (Fig. 8), where the flow direction is defined by the imbrication of the magnetic foliation (Giordano et al., 2008) due to the primary alignment of these minerals through the movement of the volcanic material over the palaeotopographical surface (e.g., Agrò et al., 2015).

The sites with the presence of SD magnetite grains must be interpreted carefully (e.g., Tarling and Hrouda, 1993; Dunlop and Ozdemir, 1997; Rochette et al., 1999; Moncinhatto et al., 2020; Pasqualon et al., 2020), since this effect generates an inverse behaviour between the magnetic and the elongation axes of magnetite, presenting K_1 perpendicular to the long axis of the grains while K_3 is parallel to it (Stephenson et al., 1986). AMS sites that exhibited this behaviour were grouped in the inverse fabric type, being proved by the comparison between the magnetic tensors of AMS and AARM (Fig. 9b and 9d), which is not affected by the SD effect (Jackson 1991). On the other hand, intermediate AMS fabrics (Fig. 9a and 9c) may arise when different mixtures of SD-MD magnetite grains occur in the same rock (Ferré, 2002; Ferré et al., 2002; Moncinhatto et al., 2020).

The flow directions obtained through the interpretations of the magnetic data are defined by two controls on the AMS of the units studied. The macroscopic control defined by the effective orientation of the main magnetic carrier that is associated with flow regimes and particle alignment (Tauxe et al., 2018) and the microscopic control directly related with the magnetic mineralogy, linked to the composition and domain structure of the particles, as previously discussed. In the stratified ignimbrites, the AMS is likely controlled by the distribution of magnetic minerals in the rock fabric, which are primarily oriented during the flow, as evidenced by the alignment and imbrication of crystals, pumices, lithic fragments and glass shards. For these deposits, the geological feature that represents the flow directions may be different for each facies due to the variations in concentrations and types of constituents. In the rheomorphic ignimbrites, the orientation of flattened pumices, marked by the eutaxitic and parataxitic texture, are the main structures that define the flow direction inferred from AMS data.

5.2. General implications: Emplacement model for volcanic deposits in TP

The correlation between AMS data and the analysis of ignimbritic facies allowed us to obtain relevant information about the mechanism of emplacement of pyroclastic-flow deposits in TP during the Acampamento Velho volcanism. The stratified ignimbrites showed sub-horizontal magnetic foliation planes, without a significant variation in dip across the different facies (e.g., variation in the content of lithic fragments and pumices). On the other hand, rheomorphic ignimbrites are characterized by a subhorizontal (Fig. 10, e.g., PT-09, 14, 15, 20, 24, 27 and 36) to mildly inclined (Fig. 10, e.g., PT-18 and 21) imbrication foliation. The predominance of subhorizontal magnetic foliation planes can be explained due to the flattening induced by strong agglutination of vitreous fragments formed by the high degree of welding of deposits (pure shear), while the mildly inclined imbrication results from a simple shear deformation produced by continued rheomorphism which increases the particle dip (Branney and Kokelaar, 1992; Kobberger and Schmincke, 1999; Sommer et al., 2013; Pueyo Anchueta et al., 2014). The high proportion of oblate ellipsoids (Table 3, $T > 0$; e.g., sites PT-05, 07, 09, 14, 18, 21 and 36) corroborates this fact, except for a few sites (PT-15, 20, 24 and 27) that may be associated with variations in the magnetic mineralogy or flow regime. These sites that showed a linear fabric also presented field flow foliations with dip $> 30^\circ$ (Fig. 10, e.g., PT-15, 24 and 27), suggesting the magnetic anisotropy in these points is not a reliable indicator of the flow structures. Works performed on welded ignimbrites attributed similarly steep inclinations of field features, such as flow foliations marked by the orientation of flattened pumices, to rheomorphism (Wang et al., 2001).

A model for the depositional system of pyroclastic flow deposits in the TP was previously discussed, based on petrogenetic and physical parameters (Sommer et al., 2011). Progressive aggradational model (Branney and Kokelaar, 1992) was adopted to explain the vertical variations in grain size, type of constituents and welding degree of deposits. The transition from stratified ignimbrites to rheomorphic suggests the persistence of high temperatures throughout the flow and the concentration of fragments with lower viscosity at the top, whose stratification

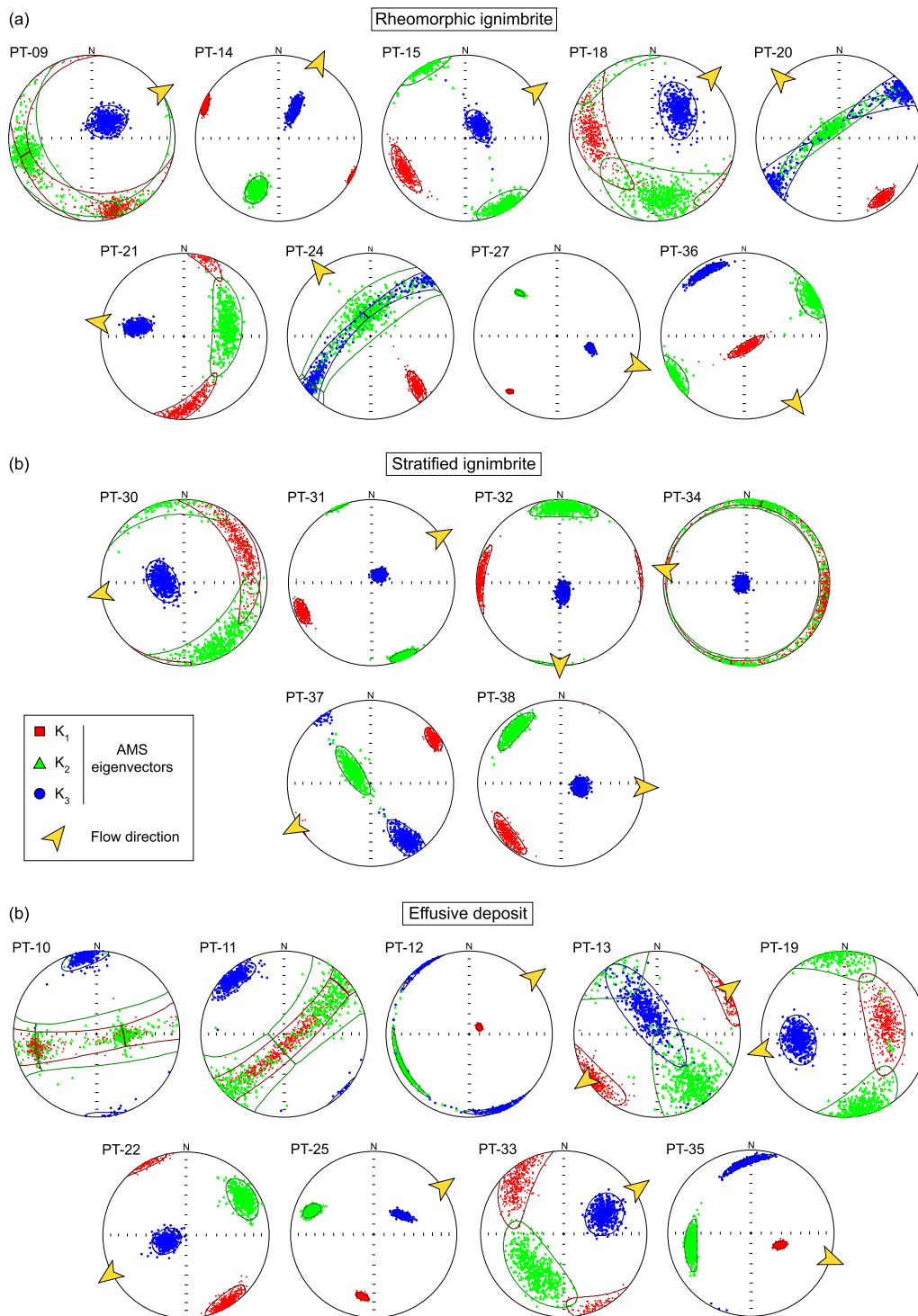


Fig. 7. Equal-area stereographic projection and their confidence zones of AMS data from rheomorphic and stratified ignimbrites and effusive deposits. The inferred flow direction based on imbrication of magnetic foliation is represented by the yellow arrow. Other AMS points collected are shown in Fig. 10b. Site locations are shown in Fig. 2.

can be explained by the variation in eruptive dynamics and short pauses of the volcanic activity (Sommer et al., 2013). This concurs with the fact that these deposits present some variations in flow directions along the vertical succession for the same spatial location (Fig. 10b). However, this transition from stratified to rheomorphic ignimbrites is marked by an erosive discordance (Fig. 3a and b), indicating a gap between the deposition of each flow. Therefore, the homogeneous aspect characteristic of this facies and the lack of evidence for significant interruptions in

the cooling history of rheomorphic ignimbrites, suggest these deposits behaved as a single cooling unit, where the flow unit was deposited rapidly one after the other. It is worth mentioning that the higher degree of welding combined with partial rheorphism indicates little loss of heating during the origin and emplacement of these flows, which is common in low-eruptive columns (e.g. Kobberger and Schmincke, 1999; Sommer et al., 2013; Costa et al., 2016; Trolese et al., 2019).

Effusive deposits present a more complex arrangement in the

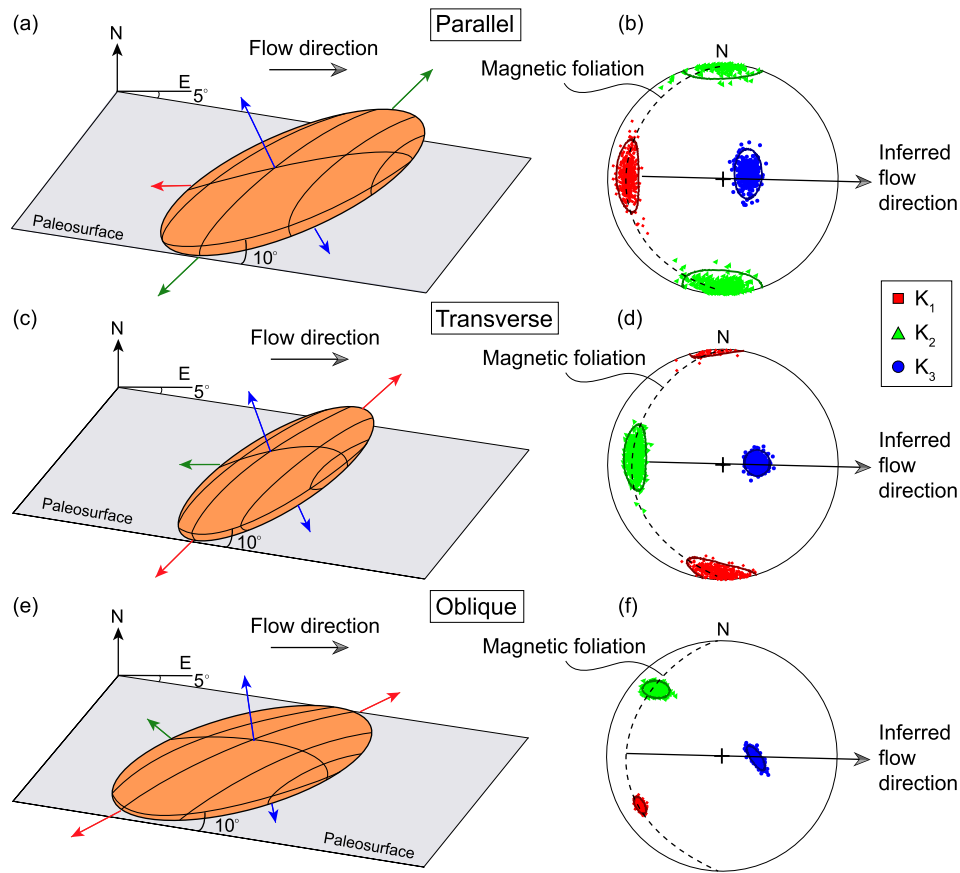


Fig. 8. Conceptual model and the related stereograms of AMS axes for imbrication of magnetic foliation found in ignimbrites, defined as parallel when K_1 is parallel to the flow direction (a-b), transverse when K_1 is orthogonal to the flow direction (c-d) and oblique when K_1 is oblique (between 35° and 55°) to the flow direction (e-f) (based on Giordano et al., 2008; Agrò et al., 2015).

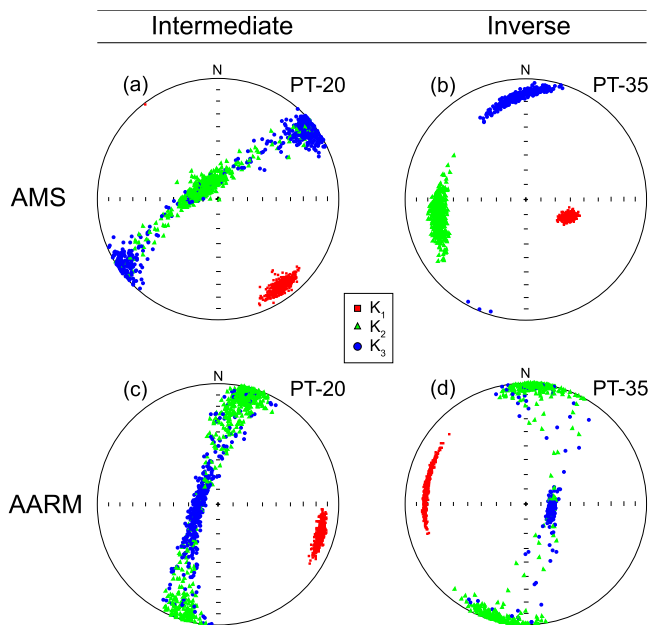


Fig. 9. Examples of intermediate and inverse magnetic fabric determined from AMS and AARM stereograms for the same sites.

evolutionary context of TP. In addition to lava flows, these deposits sometimes occur as synvolcanic bodies, whose AMS data shows a subvertical magnetic foliation (Fig. 10, e.g., sites PT-10 and 11) and

vertical field structures indicating bodies similar to cryptodomes, present in the southwestern portion of the plateau. These deposits are trachytic-rhyolitic lava flows mainly controlled by faults. There, the AMS data show a subhorizontal foliation (Fig. 10, e.g., PT-33 and 35) indicating a preferred flow direction. Based on field and geochemical data, Sommer et al. (1999) proposed the LRC may have been responsible for the formation of part of the ignimbritic deposits in TP, through a ring type conduit whose fissures are represented by the border of the complex. Geochronological and geochemical data corroborated this model, showing a cogeneticity of the AVF rocks with the LRC intrusives (Gastal, 1999; Gastal and Lafon, 2001), which were suggested as a possible source for part of the acid volcanism.

5.3. Analysis of flow directions and source identification

The directional data obtained through the AMS indicate different flow directions for the ignimbritic deposits. A more careful analysis of the spatial location, the directions of movement and the kinematic indicators present in some outcrops allows the identification of regional flow patterns in the studied units. Flow patterns include concentric (Fig. 10, e.g., sites PT-09, 14, 15, 18 and 27) and radial (Fig. 10, e.g., sites PT-01, 20, 21 and 24) flows towards the LRC borders in the southern portion of the plateau. The radial pattern occurs probably due to the effect of a ring fissure system associated to the LRC, while the concentric pattern could be related to circular fractures around the complex, which can form ridges perpendicular to the main flow direction. This would be similar to the scheme proposed by Sommer et al. (1999) to explain the relationship between the volcanic deposits of the southern portion of the TP and the intrusives of the LRC. Kobberger and Schmincke (1999) identified a similar behaviour, describing that the

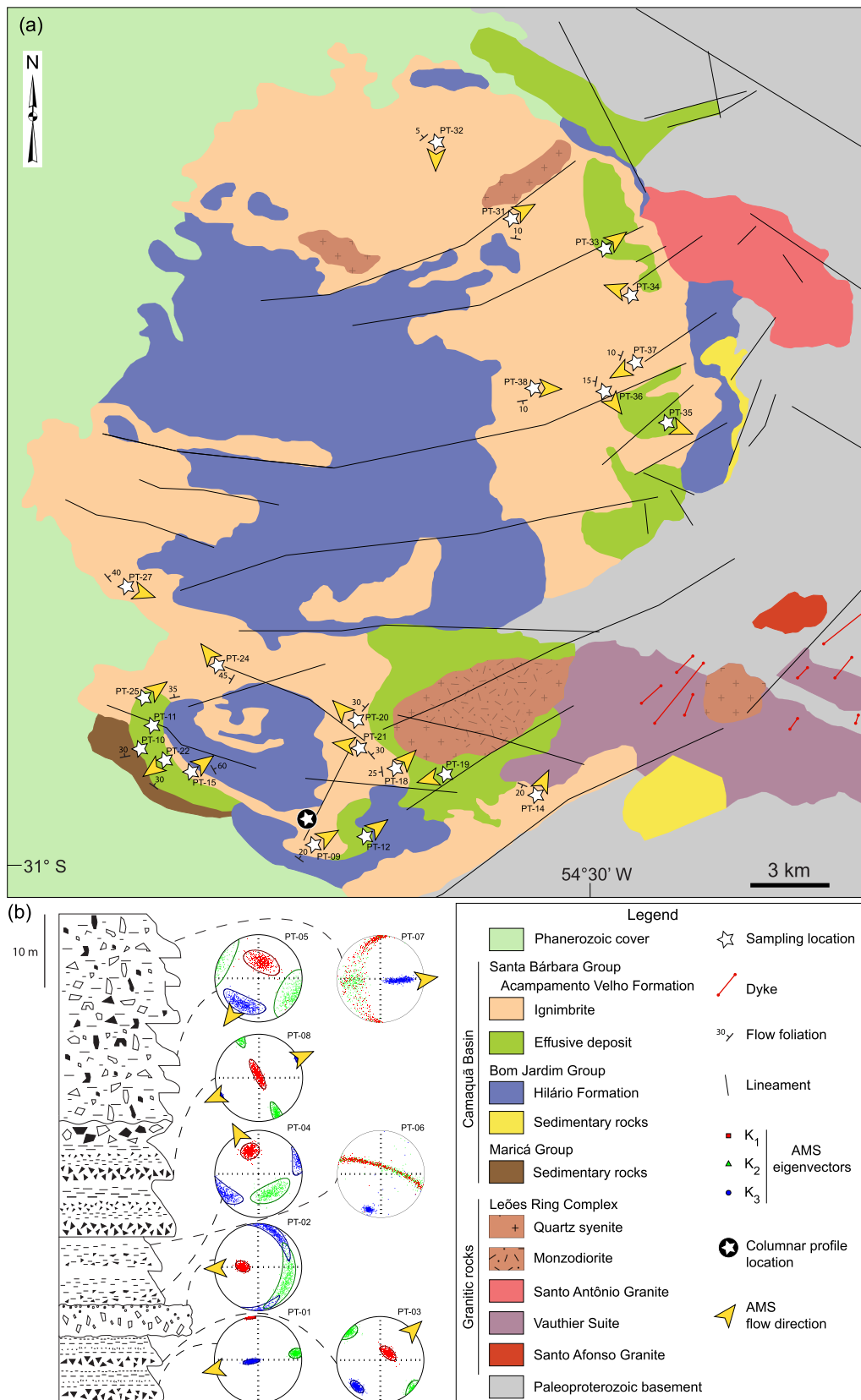


Fig. 10. Map of directional model obtained for ignimbrites and effusive deposits of Acampamento Velho volcanism in Taquarembó Plateau area (a) and the variations in the flow directions along the vertical succession represented in the columnar profile with their respective AMS stereograms (b).

pyroclastic flow is reverse but still congruent with the dip of the slope where the basement was too high to have been surmounted. Furthermore, the lineaments represented in the geological map (Figs. 2 and 10a) correspond to main fracture zones, related to brittle tectonics, possibly being fault zones. Restricted outcrops of trachytic flows show a similar behaviour to the pyroclastic deposits, with flow directions associated with ignimbrites (Fig. 10, e.g., site PT-12). Directional data in the southern portion of the TP indicate flows related to the LRC or with another volcanic source eventually located further east, outside the plateau area. The non-exposure of volcanic deposits to the east of the complex could be explained by basement uplift and the subsequent erosion since deeper intrusive bodies and, mainly, Paleoproterozoic granulitic basement outcrops next to the youngest units. As a consequence, the relationship of ignimbrites with a possible caldera linked to the LRC is complicated and requires more data.

In the northern portion of the TP, the flow directions for the ignimbrites showed a relationship with the border of the plateau, indicating a movement pattern that converges to the centre of the region (Fig. 10, e.g., sites PT-32, 34, 37 and 38). The correlation of these deposits with a complex fissure system may be linked to the genesis of these rocks, where the discontinuity with the basement may have allowed the formation of fissural conduits that feed these deposits. Although this relationship is more evident at points sampled in this area, the convergent pattern was also identified in the southern portion at the sites closest to the border of the plateau (Fig. 10, e.g., sites PT-09, 14 and 27). The occurrence of another non-outcropping volcanic structure located to the east of the northern portion, similar to the LRC, is not discarded, but there is no fieldwork evidence for this hypothesis.

5.4. Implications for Ediacaran volcanism in southernmost Brazil

The acidic volcanic rocks of the Taquarémbo plateau represent the final stages of a typically post-collisional volcano-magmatic sequence of the Brasiliano cycle of the Dom Feliciano belt (Sommer et al., 2006; Hartmann et al., 2007; Paim et al., 2014). Volcanic systems as observed in the TP, involving effusive and ignimbritic deposits with a high degree of welding and associated intrusions, are generally associated with calderas. However, there is no AMS conclusive evidence of a possible caldera related to the volcanic deposits in the TP area. Even though the directional magnetic data in the southern portion indicate flows related to the LRC, the geographic position of the complex does not justify the distribution of ignimbrite sheets all over the plateau. AMS directional data showed a correlation of these deposits with a possible fissure system, linked mainly to the borders of the plateau area. Similar acid volcanic sequences also belonging to the Ediacaran volcanism of Dom Feliciano belt were interpreted as a result of fissure systems based on faciology and volcanological aspects (Santos et al., 2019). This fissure-source model for ignimbritic deposits was applied by Aguirre-Díaz and Labarthe-Hernández (2003) to describe the formation of the Sierra Madre Occidental, the largest continuous ignimbrite province in the world (Swanson and McDowell, 1984), but is still a debated model in the literature.

Other exposures of Ediacaran volcanism of AVF rocks in Sulriograndense shield show strong similarities with the volcanic deposits of TP. The Ramada plateau, to the northeast of the study area (Fig. 1), is a direct analogue and in addition to presenting similar faciological characteristics with TP rocks, it also exhibits field relationships and compositions with intrusive bodies in the region (Sommer et al., 2013). These volcano-plutonic sequences of the Ramada plateau were interpreted as intracaldera facies, possibly originated by eruptions along ring-type fissures, in caldera systems (Sommer et al., 2011; Matté et al., 2016). Acid rocks with a similar pattern were described in the Tupanci region (Leitze et al., 2015). Despite the excellent volcanological data, there are no studies of flow dynamics, such as those provided through AMS, for these sequences. Knowledge about the magma emplacement process and the consequent reconstruction of the volcanic terrain,

interpreted by magnetic anisotropy data on a larger scale, will be useful for understanding the tectonic evolution of the Dom Feliciano belt (e.g. Xu et al., 2017; Chatterjee et al., 2018). Recent works applied this approach to study restricted outcrops of felsic lavas from AVF, demonstrating the importance of a multi-proxy analysis when dealing with ancient terrains (e.g. Haag et al., 2021).

In a broader sense, the present example shows how the magnetic anisotropy technique can be used in a complex and ancient volcanic system to better understand its dynamics and mode of emplacement. This technique has been usually applied to more recent examples, where the sources of pyroclastic deposits are still cropping out (e.g. Cagnoli and Tarling, 1997; Le Pennec et al., 1998; Palmer and MacDonald, 1999; Ort et al., 1999; LaBerge et al., 2009; Dedzo et al., 2011; Moncinhatto et al., 2020). In Precambrian terrains, the outcrops are more limited and the potential volcanic sources were likely eroded away (e.g. Haag et al., 2021). In this way, magnetic anisotropy is one of the few tools that allow one to test petrogenetic hypotheses proposed on the basis of petrochemistry, faciology and volcanological observations. In our case, the results obtained are compatible with a fissure-source model that may involve not only the area studied but also other coeval volcanic successions in the Sulriograndense shield. Potential geophysical methods (e.g. magnetometry and gravimetry) could be efficient tools to further test this interpretation of the Ediacaran volcanism in southern Brazil, through a more detailed analysis of subsurface structures (e.g. Almaguer et al., 2020).

6. Conclusion

AMS and AARM data and their kinematic indicators reported for volcanic deposits of Taquarémbo Plateau permitted to assist in the analysis and mechanisms of the emplacement of silicic units from the expressive Ediacaran volcanism in southernmost Brazil. AMS results showed different imbrication angle components between rheomorphic and stratified ignimbrites, allowing their separation in the depositional system for pyroclastic flow deposits. Magnetic mineralogy and AARM characterization were essential for the interpretation of magnetic anisotropy data, especially when SD particles dominate the magnetic fabric. AMS directional data indicates flows related to the LRC in the southern portion. However, it cannot be used to explain the distribution of ignimbrite sheets throughout the plateau area. The emplacement of pyroclastic flow deposits is probably associated with a complex fissure system, whose discontinuities with the basement at the plateau border may have served as feeder conduits for these deposits. Nevertheless, the occurrence of other non-outcropping volcanic structures located further east, outside the plateau area is not discarded. The same approach used here of a regionally distributed AMS sampling for the TP can be applied to other ancient key volcanic areas in the world, including other examples in south Brazil such as the Ramada Plateau to the northeast of the study area, which has strong similarities to the TP.

Declaration of Competing Interest

The authors declare that they have no known competing financial interests or personal relationships that could have appeared to influence the work reported in this paper.

Acknowledgements

This study was financed by the São Paulo Research Foundation, Fapesp grant 2016/06114-6. Johnathan H. Gambeta thanks the Conselho Nacional de Desenvolvimento Científico e Tecnológico (CNPq, Brazil) for the research grant and financial support. Carlos A. Sommer thanks CNPq grant (305036/2018-8, 406825/2018-6). Jairo F. Savian thanks the CNPq grant 304022/2018-7. At last, we thank Léo A. Hartmann for his support in English and figures review.

References

- Agrò, A., Zanello, E., Le Pennec, J.-L., Temel, A., 2015. Magnetic fabric of ignimbrites: A case study from the Central Anatolian Volcanic Province. *Geol. Soc. Lond.* 396 (1), 159–175.
- Aguirre-Díaz, G.J., Labarthe-Hernández, G., 2003. Fissure ignimbrites: Fissure-source origin for voluminous ignimbrites of the Sierra Madre Occidental and its relationship with Basin and Range faulting. *Geology* 31 (9), 773–776.
- Almaguer, J., Lopez-Loera, H., Macías, J.L., Saucedo, R., Yutsis, V., Guevara, R., 2020. Geophysical modeling of La Primavera caldera and its relation to volcanology activity based on 3D susceptibility inversion and potential data analysis. *J. Volcanol. Geoth. Res.* 393, 106556.
- Alva-Valdivia, L.M., Agarwal, A., Caballero-Miranda, C., García-Amador, B.I., Morales-Barrera, W., Rodríguez-Elizarraraz, S., Rodríguez-Trejo, A., 2017. Paleomagnetic and AMS studies of the El Castillo ignimbrite, central-east Mexico: Source and rock magnetic nature. *J. Volcanol. Geoth. Res.* 336, 140–154.
- Borradaile, G., 1987. Anisotropy of magnetic susceptibility: Rock composition versus strain. *Tectonophysics* 138 (2–4), 327–329.
- Branney, M.J., Kokelaar, P., 1992. A reappraisal of ignimbrite emplacement: Progressive aggradation and changes from particulate to non-particulate flow during emplacement of high-grade ignimbrite. *Bull. Volcanol.* 54 (6), 504–520.
- Cagnoli, B., Tarling, D.H., 1997. The reliability of anisotropy of magnetic susceptibility (AMS) data as flow direction indicators in friable base surge and ignimbrite deposits: Italian examples. *J. Volcanol. Geoth. Res.* 75 (3–4), 309–320.
- Cañón-Tapia, E., 2004. Flow direction and magnetic mineralogy of lava flows from the central parts of the peninsula of Baja California, Mexico. *Bull. Volcanol.* 66 (5), 431–442.
- Cañón-Tapia, E., Mendoza-Borunda, R., 2014. Magnetic petrofabric of igneous rocks: Lessons from pyroclastic density current deposits and obsidians. *J. Volc. Geotherm. Res.* 289, 151–169.
- Cerva-Alves, T., Hartmann, L.A., Remus, M.V.D., Lana, C., 2020. Integrated ophiolite and arc evolution, southern Brazilian Orogen. *Precamb. Res.* 341, 105648.
- Chadima, M., Cajz, V., Tycová, P., 2009. On the interpretation of normal and inverse magnetic fabric in dikes: Examples from the Eger Graben, NW Bohemian Massif. *Tectonophysics* 466 (1–2), 47–63.
- Chatterjee, S., Mondal, S., Gain, D., Baidya, T.K., Mazumdar, D., 2018. Interpretation of magnetic fabrics in the Dalma volcanic rocks and associated meta-sediments of the Singbhum Mobile Belt. *J. Earth Syst. Sci.* 127 (6), 1–18.
- Chemale Jr, F., 2000. Evolução geológica do Escudo Sul-rio-grandense. In: Holz, M., De Ros, L.F. (Eds.), *Geologia do Rio Grande do Sul*. CIGO/UFRGS, Porto Alegre, 13–52.
- Costa, A., Suzuki, Y.J., Cerminara, M., Devenish, B.J., Ongaro, T.E., Herzog, M., Van Eaton, A.R., Denby, L.C., Bursik, M., Vittori, M.M., Engwell, S., 2016. Results of the eruptive column model inter-comparison study. *J. Volcanol. Geoth. Res.* 326, 2–25.
- Dedzo, M.G., Nédélec, A., Nono, A., Njanko, T., Font, E., Kamgang, P., Njonfang, E., Launeau, P., 2011. Magnetic fabrics of the Miocene ignimbrites from West-Cameroun: Implications for pyroclastic flow source and sedimentation. *J. Volcanol. Geoth. Res.* 203 (3–4), 113–132.
- Deng, C., Zhu, R., Jackson, M.J., Verosub, K.L., Singer, M.J., 2001. Variability of the temperature-dependent susceptibility of the Holocene Eolian deposits in the Chinese loess plateau: A pedogenesis indicator. *Phys. Chem. Earth Part A* 26 (11–12), 873–878.
- Dunlop, D.J., Özdemir, Ö., 1997. *Rock Magnetism: Fundamentals and Frontiers*. Cambridge University Press, Cambridge.
- Ferré, E.C., 2002. Theoretical models of intermediate and inverse AMS fabrics. *Geophys. Res. Lett.* 29 (7), 31–1.
- Ferré, E.C., Bordarier, C., Marsh, J.S., 2002. Magma flow inferred from AMS fabrics in a layered mafic sill, Insiwza, South Africa. *Tectonophysics* 354 (1–2), 1–23.
- Fisher, R.V., Orsi, G., Ort, M.H., Heiken, G., 1993. Mobility of a large-volume pyroclastic flow- emplacement of the Campanian Ignimbrite, Italy. *J. Volcanol. Geoth. Res.* 56 (3), 205–220.
- Fragoso-Cesar, A.R.S., Fambri, G.L., Paes de Almeida, R., Pelosi, A.P.M.R., Janikian, L., Riccomini, C., Machado, R., Nogueira, A.C.R., Saes, G.S., 2000. The Camaquã Extensional Basin: Neoproterozoic-Early Paleozoic Transition in the State of Rio Grande do Sul, Brazil. *Rev. Brasileira de Geociências* 30 (3), 438–441.
- Gastal, M.C.P., 1999. The alkaline and shoshonitic intrusives in the region of the Taquarém Plateau, southern Brazil: Are they genetically related? *Revista Brasileira de Geociências* 29 (1), 85–98.
- Gastal, M.C.P., Lafon, J.M., 2001. Novas idades $^{207}\text{Pb}/^{206}\text{Pb}$ e geoquímica isotópica Nd-Sr para granitóides shoshoníticos e alcalinos das regiões de Lavras do Sul e Taquarém, RS. VIII Congresso Brasileiro de Geoquímica 21–26.
- Giordano, G., Porreca, M., Musacchio, P., Mattei, M., 2008. The Holocene Secche di Lazzaro phreatomagmatic succession (Stromboli, Italy): evidence of pyroclastic density current origin deduced by facies analysis and AMS flow directions. *Bull. Volcanol.* 70 (10), 1221–1236.
- Graham, J.W., 1954. Magnetic anisotropy, an unexploited petrofabric element. *Geol. Soc. Am. Bull.* 65, 1257–1258.
- Haag, M.B., de Freitas, R.B., Sommer, C.A., Savian, J.F., Lima, E.F., Gambeta, J.H., Lyra, D.S., Trindade, R.I.F., 2021. Multi-proxy case study of a Neoproterozoic rhyolite flow in southernmost Brazil: Emplacement mechanisms and implications for ancient felsic lavas. *J. S. Am. Earth Sci.* 107, 102982.
- Harrison, R.J., Feinberg, J.M., 2008. FORCinel: An improved algorithm for calculating first-order reversal curve distributions using locally weighted regression smoothing. *Geochem. Geophys. Geosyst.* 9 (5).
- Hartmann, L.A., Chemale Jr, F., Philipp, R.P., 2007. Evolução geotectônica do Rio Grande do Sul no pré-cambriano. In: Iannuzzi R., Frantz J.C., (Eds.), (50), 97–123.
- Incoronato, A., Addison, F.T., Tarling, D.H., Nardi, G., Pescatore, T., 1983. Magnetic fabric investigations of pyroclastic deposits from Phlegrean Fields, southern Italy. *Nature* 306 (5942), 461–463.
- Jackson, M., 1991. Anisotropy of magnetic remanence: a brief review of mineralogical sources, physical origins and geological applications, and comparison with susceptibility anisotropy. *Pure Appl. Geophys.* 136, 1–28.
- Janikian, L., Almeida, R.P., Trindade, R.I.F., Fragoso-Cesar, A.R.S., D'Agrella-Filho, M.S., Dantas, E.L., Tohver, E., 2008. The continental record of Ediacaran volcano-sedimentary successions in southern Brazil and their global implications. *Terra Nova*, 20(4), 259–266.
- Jelinek, V., 1978. Statistical processing of anisotropy of magnetic susceptibility measured on groups of specimens. *Stud. Geophys. Geod.* 22 (1), 50–62.
- Jelinek, V., 1981. Characterization of the magnetic fabric of rocks. *Tectonophysics* 79 (3–4), 563–567.
- Jousset, P., Pallister, J., Boichu, M., Buongiorno, M.F., Budisantoso, A., Costa, F., Andreastuti, S., Prata, F., Schneider, D., Clarisse, L., Humaida, H., 2012. The 2010 explosive eruption of Java's Merapi volcano—a '100-year' event. *J. Volcanol. Geoth. Res.* 241, 121–135.
- Kobberger, G., Schmincke, H.U., 1999. Deposition of rheomorphic ignimbrite D (Mogán Formation), Gran Canaria, Canary Islands, Spain. *Bull. Volcanol.* 60 (6), 465–485.
- LaBerge, R.D., Porreca, M., Mattei, M., Giordano, G., Cas, R.A.F., 2009. Meandering flow of a pyroclastic density current documented by the anisotropy of magnetic susceptibility (AMS) in the quartz latite ignimbrite of the Pleistocene Monte Cimino volcanic centre (central Italy). *Tectonophysics* 466, 64–78.
- Leite, F.P., Sommer, C.A., Lima, E.F., Matté, V., 2015. O vulcanismo alta-silica da região do Tupancí, NW do Escudo Sul-Rio-Grandense: faciologia, petrografia e litológica. *Pesquisas em Geociências* 42, 5–24.
- Le Pennec, J.-L., Chen, Y., Diot, H., Froger, J.-L., Gourgaud, A., 1998. Interpretation of anisotropy of magnetic susceptibility fabric of ignimbrites in terms of kinematic and sedimentological mechanisms: An Anatolian case-study. *Earth Planet. Sci. Lett.* 157 (1), 105–127.
- Lima, E.F., Sommer, C.A., Nardi, L.V.S., 2007. O vulcanismo Neoproterozoico Ordoviciano no Escudo Sul-rio-grandense: os ciclos vulcânicos da Bacia do Camaquã. In: Iannuzzi R. & Frantz J.C. (eds.), 50, 79–95.
- Lima, E.F., Waichel, B.L., Rossetti, L.D.M.M., Sommer, C.A., Simões, M.S., 2018. Feeder systems of acidic lava flows from the Paraná-Etendeka Igneous Province in southern Brazil and their implications for eruption style. *J. S. Am. Earth Sci.* 81, 1–9.
- Magge, C., O'Driscoll, B., Petronis, M., Stevenson, C., 2016. Three-dimensional magma flow dynamics within subvolcanic sheet intrusions. *Geosphere* 12 (3), 842–866.
- Matté, V., Sommer, C.A., Lima, E.F., Philipp, R.P., Basei, M.A.S., 2016. Post-collisional Ediacaran volcanism in oriental Ramada Plateau, southern Brazil. *J. S. Am. Earth Sci.* 71, 201–222.
- Moncinhatto, T.R., Haag, M.B., Hartmann, G.A., Savian, J.F., Poletti, W., Sommer, C.A., Caselli, A.T., Trindade, R.I.F., 2020. Mineralogical control on the magnetic anisotropy of lavas and ignimbrites: A case study in the Cavihue-Copahue field (Argentina). *Geophys. J. Int.* 220, 821–838.
- Newhall, C.G., Bronto, S., Alloway, B., Banks, N.G., Bahar, I., Del Marmol, M.A., Hadisantonio, R.T., Holcomb, R.T., McGeehin, J., Miksic, J.N., Rubin, M., 2000. 10,000 Years of explosive eruptions of Merapi Volcano, Central Java: archaeological and modern implications. *J. Volcanol. Geoth. Res.* 100 (1–4), 9–50.
- Ort, M.H., 1993. Eruptive processes and caldera formation in a nested down-sag-collapse caldera: Cerro Panizos, central Andes Mountains. *J. Volcanol. Geoth. Res.* 56 (3), 221–252.
- Ort, M.H., Rosi, M., Anderson, C.D., 1999. Correlation of deposits and vent locations of the proximal Campanian Ignimbrite deposits, Campi Flegrei, Italy, based on natural remanent magnetization and anisotropy of magnetic susceptibility characteristics. *J. Volcanol. Geoth. Res.* 91 (2–4), 167–178.
- Paim, P.S.G., Chemale Jr, F., Lopes, R.C., 2000. A Bacia do Camaquã. In: Holz, M., De Ros, L.F. (Eds.), *Geologia do Rio Grande do Sul*. CIGO/UFRGS, Porto Alegre, 231–274.
- Paim, P.S.G., Junior, F.C., Wildner, W., 2014. Estágios evolutivos da Bacia do Camaquã (RS). *Ciência e Natura* 36 (3), 183–193.
- Palmer, H.C., MacDonald, W.D., 1999. Anisotropy of magnetic susceptibility in relation to source vents of ignimbrites: Empirical observations. *Tectonophysics* 307 (1–2), 207–218.
- Pasqualon, N.G., Savian, J.F., Lima, E.F., Luz, F.R., Moncinhatto, T.R., Trindade, R.I.F., 2020. Emplacement dynamics of alkaline volcanic and subvolcanic rocks in Trindade Island, Brazil. *J. Volcanol. Geoth. Res.* 406, 107078 <https://doi.org/10.1016/j.jvolgeores.2020.107078>.
- Petrovský, E., Kapička, A., 2006. On determination of the Curie point from thermomagnetic curves. *J. Geophys. Res.* 111 (B12).
- Philipp, R.P., Pimentel, M.M., Chemale Jr, F., 2016. Tectonic evolution of the Dom Feliciano Belt in Southern Brazil: Geological relationships and U-Pb geochronology. *Braz. J. Geol.* 46, 83–104.
- Potter, D.K., Stephenson, A., 1988. Single-domain particles in rocks and magnetic fabric analysis. *Geophys. Res. Lett.* 15 (10), 1097–1100.
- Pueyo Anchueta, Ó., Imaz, A.G., Gil-Peña, I., Maestro, A., Galindo-Zaldívar, J., López-Martínez, J., Rey, J., Soto, R., Oliva-Urcia, B., 2014. Application of AMS for reconstruction of the geological evolution of recent volcanic systems: Case of Deception Island (South Shetland Islands, Antarctica). *Tectonophysics* 626, 69–85.
- Ribeiro, M., Fantinel, L.M., 1978. Associações petrotectônicas do Escudo Sul-rio-grandense: I tabulação e distribuição das associações petrotectônicas do escudo do Rio Grande do Sul. *Ilheringia, Série Geológica* 5, 19–54.
- Roberts, A.P., Cui, Y., Verosub, K.L., 1995. Wasp-waisted hysteresis loops: Mineral magnetic characteristics and discrimination of components in mixed magnetic systems. *J. Geophys. Res. Solid Earth* 100 (B9), 17909–17924.

- Roberts, A.P., Pike, C.R., Verosub, K.L., 2000. First-order reversal curve diagrams: A new tool for characterizing the magnetic properties of natural samples. *J. Geophys. Res. Solid Earth* 105 (B12), 28461–28475.
- Roberts, A.P., Heslop, D., Zhao, X., Pike, C.R., 2014. Understanding fine magnetic particle systems through use of first-order reversal curve diagrams. *Rev. Geophys.* 52, 557–602.
- Roberts, A.P., Tauxe, L., Heslop, D., Zhao, X., Jiang, Z., 2018. A critical appraisal of the “Day” diagram. *J. Geophys. Res. Solid Earth* 123, 2618–2644. <https://doi.org/10.1002/2017JB015247>.
- Rochette, P., Jackson, M., Aubourg, C., 1992. Rock magnetism and the interpretation of anisotropy of magnetic susceptibility. *Rev. Geophys.* 30 (3), 209–226.
- Rochette, P., Aubourg, C., Perrin, M., 1999. Is this magnetic fabric normal? A review and case studies in volcanic formations. *Tectonophysics* 307 (1–2), 219–234.
- Santos, E.A.D., Sommer, C.A., Waichel, B.L., Haag, M.B., 2019. Ediacaran post-collisional high-silica volcanism associated to the Florianópolis Batholith, Dom Feliciano Belt, southernmost Brazil: Lithofacies analysis and petrology. *J. S. Am. Earth Sci.* 96, 102299.
- Sommer, C.A., Lima, E.F., Nardi, L.V.S., 1999. Evolução do vulcanismo alcalino da porção sul do platô do taquarombó, Dom Pedrito - RS. *Revista Brasileira de Geociências* 29 (2), 245–254.
- Sommer, C.A., Lima, E.F., Nardi, L.V.S., Figueiredo, A.M.G., Pierosan, R., 2005. Potassic and low-and high-Ti mildly alkaline volcanism in the Neoproterozoic Ramada Plateau, southernmost Brazil. *J. S. Am. Earth Sci.* 18 (3–4), 237–254.
- Sommer, C.A., Lima, E.F., Nardi, L.V.S., Liz, J.D., Waichel, B.L., 2006. The evolution of Neoproterozoic magmatism in southernmost Brazil: Shoshonitic, high-K, tholeiitic and silica-saturated, sodic alkaline volcanism in post-collisional basin. *Anais da Academia Brasileira de Ciências* 78 (3), 573–589.
- Sommer, C.A., Lima, E.F., Pierosan, R., Machado, A., 2011. Reoignimbritos e ignimbritos de alto grau do vulcanismo Acampamento Velho, RS: origem e temperatura de formação. *Revista Brasileira de Geociências* 41 (3), 420–435.
- Sommer, C.A., Lima, E.F., Machado, A., Rossetti, L.D.M.M., Pierosan, R., 2013. Recognition and characterisation of high-grade ignimbrites from the neoproterozoic rhyolitic volcanism in southernmost Brazil. *J. S. Am. Earth Sci.* 47, 152–165.
- Stephenson, A., Sadikun, S.T., Potter, D., 1986. A theoretical and experimental comparison of the anisotropies of magnetic susceptibility and remanence in rocks and minerals. *Geophys. J. Int.* 84 (1), 185–200.
- Swanson, E.R., McDowell, F.W., 1984. Calderas of the Sierra Madre Occidental volcanic field western Mexico. *J. Geophys. Res. Solid Earth* 89 (B10), 8787–8799.
- Tarling, D.H., Hrouda, F., 1993. In: *The Magnetic Anisotropy of Rocks*. Chapman & Hall, London, p. 217.
- Tauxe, L., Kylstra, N., Constable, C., 1991. Bootstrap statistics for paleomagnetic data. *J. Geophys. Res.* 96 (B7), 11723–11740.
- Tauxe, L., Mullender, T.A.T., Pick, T., 1996. Potbellies, waist-waists, and superparamagnetism in magnetic hysteresis. *J. Geophys. Res.* 101 (B1), 571–583.
- Tauxe, L., Banerjee, S. K., Butler, R. F., Van der Voo, R., 2018. *Essentials of paleomagnetism*, 5th web edition.
- Troise, M., Germinara, M., Ongaro, T.E., Giordano, G., 2019. The footprint of column collapse regimes on pyroclastic flow temperatures and plume heights. *Nat. Commun.* 10 (1), 1–10.
- Wang, X., Roberts, J., Schmidt, P., 2001. Flow directions of Carboniferous ignimbrites, southern New England Orogen, Australia, using anisotropy of magnetic susceptibility. *J. Volcanol. Geoth. Res.* 110 (1–2), 1–25.
- Wiegand, M., Trumbull, R.B., Kontny, A., Greiling, R.O., 2017. An AMS study of magma transport and emplacement mechanisms in mafic dykes from the Etendeka Province, Namibia. *Tectonophysics* 716, 149–167.
- Wildner, W., Nardi, L.V.S., Lima, E.F., 1999. Post-collisional alkaline magmatism on the Taquarombó plateau: a well-preserved Neoproterozoic-Cambrian Plutono-volcanic association in southern Brazil. *Int. Geol. Rev.* 41 (12), 1082–1098.
- Wildner, W., Lima, E.F., Nardi, L.V.S., Sommer, C.A., 2002. Volcanic cycles and setting in the Neoproterozoic III to Ordovician Camaquã Basin succession in southern Brazil: characteristics of post-collisional magmatism. *J. Volcanol. Geoth. Res.* 118 (1–2), 261–283.
- Xu, H., Yang, Z., Peng, P., Ge, K., Jin, Z., Zhu, R., 2017. Magnetic fabrics and rock magnetism of the Xiong'er volcanic rocks and their implications for tectonic correlation of the North China Craton with other crustal blocks in the Nuna/Columbia supercontinent. *Tectonophysics* 712, 415–425.